Bis (α-iminopyridine) Stabilized Dimeric Sb(II) and Bi(II) Tetra-cation : Bond Lability Based Reactivity

A Thesis

submitted to

Indian Institute of Science Education and Research Pune

in partial fulfilment of the requirements for the

BS-MS Dual Degree Programme

by

Hritwik Haldar

(20191151)

Indian Institute of Science Education and Research Pune

Dr. Homi Bhabha Road,

Pashan, Pune 411008, INDIA.

March, 2024

Supervisor: Dr. Moumita Majumdar

Student: Hritwik Haldar

Certificate

This is to certify that this dissertation entitled **Bis (α-iminopyridine) Stabilized Dimeric Sb(II) and Bi(II) Tetracation : Bond Lability Based Reactivity** towards the partial fulfillment of the BS-MS dual degree programme at the Indian Institute of Science Education and Research, Pune represents research work carried out by **Hritwik Haldar** (20191151) at Indian Institute of Science Education and Research under the supervision of **Dr. Moumita Majumdar**, Associate Professor, Department of Chemistry, during the academic year 2023-2024.

Moumita Majumdar

Dr. Moumita Majumdar

Supervisor

Committee:

Name of your Guide: Dr. Moumita Majumdar

Name of Your TAC: Dr. Debangsu Sil

This thesis is dedicated to my family, friends, and lab members

Declaration

I hereby declare that the matter embodied in the report entitled **Bis (α-iminopyridine) Stabilized Dimeric Sb(II) and Bi(II) Tetracation : Bond Lability Based Reactivity** are the results of the work carried out by me at the Department of Chemistry, Indian Institute of Science Education and Research, Pune, under the supervision of Dr. Moumita Majumdar and the same has not been submitted elsewhere for any other degree.

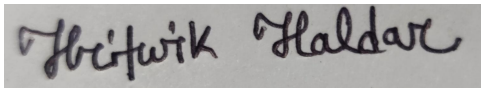

Hritwik Haldar

Date: 15/03/2024

Table of Contents

List of Tables

List of Figures

Abstract

Bis(α-iminopyridine) stabilized distibane tetra-cationic **[1]$_2$** and dibismuthane tetra-cationic **[2]$_2$** compounds have been synthesized. Both the compounds have been characterized in the solid-state using single-crystal X-ray diffraction and NMR techniques in the solution state. These dimeric species exist in equilibrium with their monomeric radical species which have been characterized using EPR techniques and absorption spectroscopy. Furthermore, reactivity study of **[1]$_2$** have been performed with O_2, E_2Ph_2 (E = S, Se), 1,4-benzoquinone, and TEMPO giving compounds **3**-**6**. All the compounds have been characterized using multinuclear NMR spectroscopy and single crystal X-ray diffraction analysis. The formation of compounds **3**-**6** confirm the homolytic cleavage of **[1]$_2$** in the solution. The bonding features of **[1]$_2$** and **[2]$_2$** have been established through computational study.

Acknowledgments

I would like to express my sincere gratitude to Dr. Moumita Majumdar, my thesis supervisor, for granting me the opportunity to work in her lab and for creating an exceptional research atmosphere in the lab. Her guidance and support throughout my MS thesis project have been pivotal in shaping my academic journey. I am also deeply thankful to Dr. Debangsu Sil, my TAC member, for his invaluable feedback and suggestions, which greatly contributed to the enhancement of my research work.

I extend my appreciation to the Department of Chemistry at IISER Pune for providing an outstanding research environment even at undergraduate level, along with access to excellent NMR and XRD facilities. My heartfelt thanks go out to my family, friends (Ranojoy, Ankan, Soumya, Shayandeep, Rahul Da, Souvik Da, Soumya Da, Panja, Pritam) and my life partner Aritrika for their continuous support during the challenging phases of my academic pursuit. Furthermore, I am indebted to my lab partners for their assistance and valuable insights that helped my project significantly.

I also wish to express my gratitude to Dr. Cem B. Yildiz, my computational collaborator, for providing NBO and spin density data. Lastly, I express my gratitude to KVPY for their financial support through their fellowship program, which played a crucial role in facilitating my academic endeavors.

Chapter 1 Introduction

Understanding the bonding scenario in main group homo-metallic bonds continue to challenge our knowledge of the nature of chemical bond. In the last few decades, there have been several landmark discoveries along this direction. A few prominent ones are the lightest homo-metallic bond in the solid state Be(I)-Be(I) dimer [1], the Mg(I)-Mg(I) dimer [2], heavier analogues (Ge, Sn, Pb) of alkenes and alkynes [3], homo-atomic double bonds between heavier group 15 and 13 elements [4]. These metal–metal bonded systems are increasingly finding applications in fields as diverse as reducing agents [5], small molecule activation and organometallic catalysis [6].

In general, the formation of metal-metal bond is a delicate balance between the diffused nature of the metal valence orbitals to engage in suitable diatomic overlap on one hand and avoiding competitive interference from small molecules (water, solvent and dioxygen) on the other hand.[7] Generally, sterically encumbered ligands are used to kinetically stabilize main group metal-metal bonds from the competitive interference of these small molecules.[7] In the main group metal-metal bonds, the valence orbitals ns and/or np participate in bonding. For, s block elements it is predominantly ns orbital that participate in bonding. For example, computational studies show that the Mg-Mg bond in β-diketiminate-chelated magnesium(I) dimer has 90% 3s character.[2] And for heavier main group elements, ns orbitals become non-bonding due to the pronounced inert-pair effect. So, only np orbital participates in bonding. For example, $Ph_2Sb\text{-}SbPh_2$ has 95% p character in the Sb-Sb bond.[8] The strength of main group metal-metal bond is dependent on the principal quantum number (n) of the main group element's valence orbital. With increasing principal quantum number, the diffuse nature of the orbital increases which leads to inefficient overlap and subsequently weakens metal-metal bond.[7]

Although, bonding and reactivities of doubly bonded heavier pnictogens (dipnictenes, Pn = Sb, Bi) are well documented in the literature,[9] the chemistry of heavier singly bonded dipnictanes is less popularly known. Dipnictanes ($R_2Pn\text{-}PnR_2$, Pn = N - Bi) contain Pn-Pn single bond where Pn has an oxidation state of +II. The most basic representation for this category of compounds are the antimony and bismuth analogues of tetraalkyl or tetraaryl hydrazines. The first reported dipnictane, Me_4As_2, which is also known as "*Cadet's fuming arsenical liquid*" or "*Cacodyl*" was prepared by Louis Cadet de Gassicourt in 1760 which was further investigated by Robert Wilhelm Bunsen.[10] However, the Pn = Sb, Bi analogue

of "*Cacodyl*", known as tetramethyldistibanes (Me_4Sb_2) and tetramethyldibismuthanes (Me_4Bi_2) respectively, were first reported in the early 1930s.[11] They were synthesized by reaction of methyl radicals with mirrors of elemental Sb and Bi. Subsequently, starting in the 1980s, efficient methods for synthesizing alkyl and aryl substituted distibanes and dibismuthanes (R_4Pn_2, Pn = Sb, Bi) (**I**) (Figure 1) were developed, leading to detailed investigations into their structures and chemical reactivity.[12] During this period the first crystal structures of distibanes and dibismuthanes were unveiled which confirms the presence of Pn-Pn covalent bond in the distibanes and dibismuthanes.[13]

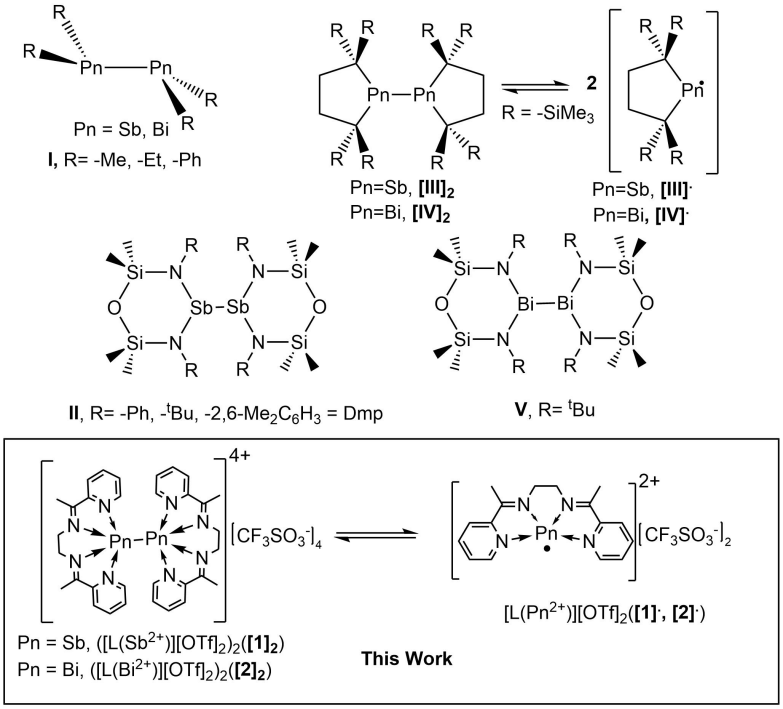

Figure 1. I) Neutral distibanes and dibismuthanes where R= -Me, -Et, -Ph; **II**) Neutral distibane supported by bulky bis(amidodimethyl)disiloxane ligands $[O(SiMe_2NR)_2]^{2-}$ ($[NON^R]^{2-}$) where R= -Ph, -^{t}Bu, -2,6-$Me_2C_6H_3$ = Dmp; **[III]$_2$, [IV]$_2$**) Neutral distibane and dibismuthane stabilized with bulky bidentate alkyl ligand 1,1,4,4-tetrakis-(trimethylsilyl)butane-1,4-diyl ligand which generates Sb(II) (**[III]**·) and Bi(II) (**[IV]**·) radicals respectively in solution state; **V**) Neutral sterically hindered dibismuthane supported by bis(amidodimethyl)disiloxane ligands $[O(SiMe_2NR)_2]^{2-}$ ($[NON^R]^{2-}$) where R= -^{t}Bu; **This Work**.

Many synthetic approaches have been explored to synthesize heavier dipnictanes. The most common method involves the generation of sodium salt of diorganyl stibide or bismuthide followed by oxidative coupling in the presence of 1,2-dichloroethane. This procedure was first used by Notles and co-workers [14] in the 1970s for the synthesis of Et_4Sb_2, which was later extended by Ashe and co-workers [15] in the synthesis of tetramethyldibismuthanes Me_4Bi_2. Notably, direct reduction of R_2Pn-X (X = Halides) into corresponding dipnictanes using metallic reducing agents like magnesium [16], KC_8 [17] Mg(I)-Mg(I) dimer [18] etc. has been achieved. This eliminates the necessity of the sodium-

pnictide pathway. A less commonly explored method for forming Pn-Pn (Pn = Sb, Bi) bonds involves dehydro-coupling (H_2 elimination).[19]

Distibanes and dibismuthanes generally contain very weak covalent bond which is due to inefficient overlap between the two 5p orbitals and two 6p orbitals respectively. Thus they have been used as a starting material for the synthesis of Sb- and Bi- centered persistent radicals.[17] Introducing steric bulk in the system further weakens the bond.[18] Martyn P. Coles and coworkers have reported a set of distibanes (**II**) and dibismuthane (**V**)[21] (Figure 1) supported by bis(amidodimethyl)disiloxane ligands $[O(SiMe_2NR)_2]^{2-}$ ($[NON^R]^{2-}$) where they varied the R groups (R = Ph, ^{t}Bu, 2,6-$Me_2C_6H_3$ = Dmp) and shown that with increasing steric bulk in the system Sb-Sb bond length increases from Ph to Dmp for the distibane (**II**).[18] Having R = Dmp, Sb-Sb bond length is 3.0352(5) Å which far exceeds the sum of the molecular single-bond covalent radii ($\sum_{(Sb\text{-}Sb)}$ =2.80 Å).[20] Subsequently, it is the most reactive among all of them and displays a degree of radical character in solution state which was characterized by TD-DFT calculations and UV-Vis spectroscopy. This R = Dmp analogue can activate white phosphorus (P_4) by breaking the P-P covalent bond.[18] The first persistent antimony(II) and bismuth(II)-centered radical in solution state were reported by Iwamoto and co-workers where they first isolated a distibane (**[III]$_2$**) and dibismuthane (**[IV]$_2$**)[17] (Figure 1) using bulky bidentate alkyl ligand 1,1,4,4-tetrakis-(trimethylsilyl)butane-1,4-diyl. Due to high steric bulk, **[III]$_2$** and **[IV]$_2$** has exceptionally long Sb-Sb bond of 3.0297(4) Å and Bi-Bi bond of 3.1831(3) Å which far exceed the sum of the Sb-Sb single-bond and Bi-Bi single-bond covalent radii (molecular single-bond covalent radii ($\sum_{(Bi\text{-}Bi)}$ =3.02 Å)[20]. Due to this labile nature, in the solution state the Sb-Sb bond and Bi-Bi bond present in **[III]$_2$** and **[IV]$_2$** respectively homolytically break and generate persistent antimony(II) and bismuth(II)-centred radical (**[III]**·) and (**[IV]**·) which is characterized by EPR (for only **[III]**·), UV-Vis and NMR spectroscopy. Later, similar works have led to isolation of antimony(II) and bismuth(II)-centered radicals.[22]

While several neutral heavier dipnictanes have been reported in recent literatures, the synthesis of single-bonded cationic antimony or bismuth dimers, referred to as cationic heavier dipnictanes remains unreported. As a matter of fact, there are only very few reports of cationic dimers (Figure 2) in main group chemistry literature.[23] Schulz and coworkers recently achieved stabilization of heavier dipnictene di-cations (Pn = Sb, Bi) using Ga(I)-based ligand.[23a] Additionally, Krossing and co-workers isolated di-cationic digallene and diindene employing a bisphosphine ligand.[23b] The same group also reported di-cationic digallanes stabilized with a mesityl-substituted β-diketiminate

([NacNac^{Mes}]$^{-}$) ligand, initiating from a Ga(I)$^{+}$ cation precursor which disproportionated in the presence of the ligand, yielding a di-cationic gallium dimer stabilized with [NacNacMes]$^{-}$ ligand.[23c] Recently, Driess and coworkers reported a di-cationic Ge dimer, wherein they initially stabilized germylone Ge(0) using bis(silylenyl) *ortho*-dicarborane ligand, which upon one-electron oxidation generated a di-cationic bis(silylene)-supported Ge_2 dimer using $[Cp_2Fe][B\{C_6H_3(CF_3)_2\}_4]$.[23d] Notably, all reported cationic main group dimers are di-cationic, highlighting a gap in the field of main group chemistry for tetra-cationic single bonded dimers.

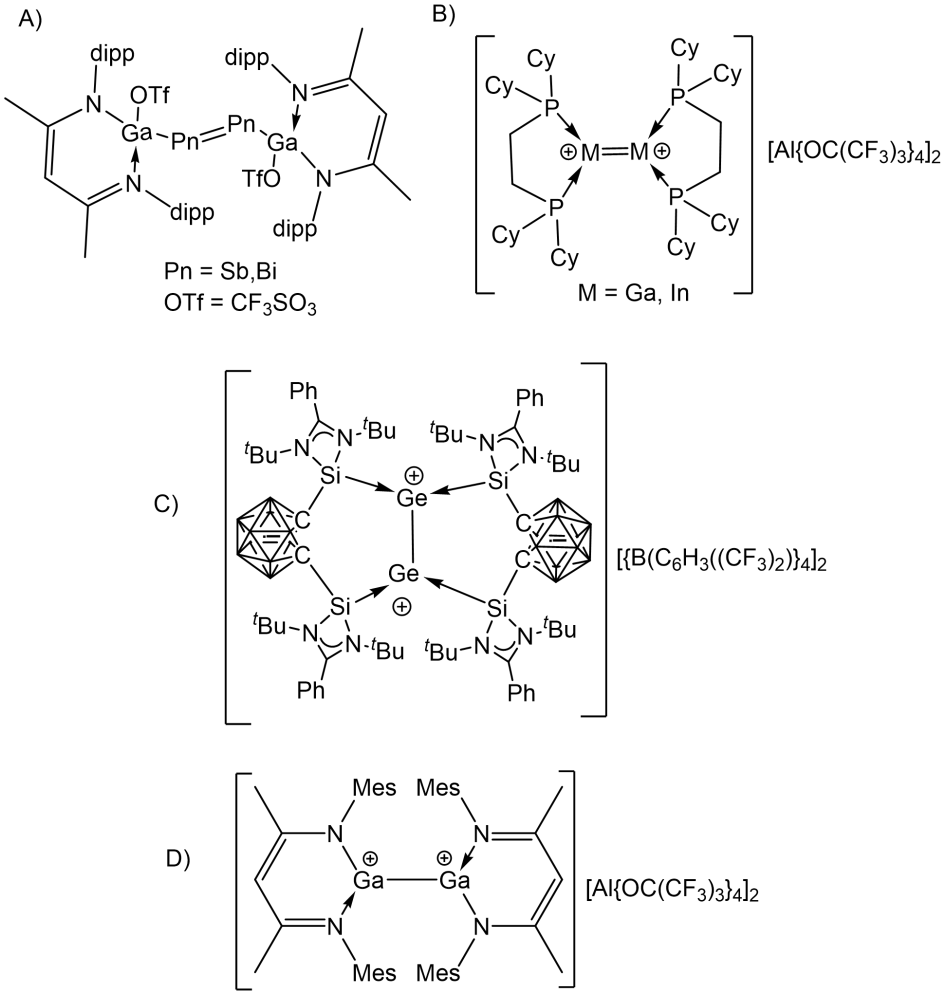

Figure 2. Reported main group cationic dimers - A) Ga(I)-based ligand stabilized di-cationic distibene and dibismuthene; B) Bisphosphine ligand stabilized di-cationic digallene and diindene; C) bis(silylenyl) *ortho*-dicarborane ligand supported di-cationic Ge dimer; D) [NacNac^{Mes}]$^{-}$ ligand stabilized di-cationic gallium dimer.

In this thesis work, we have employed the bis(α-iminopyridine) ligand (**L**) to stabilize the first reported tetra-cationic single bonded antimony and bismuth dimer. In our group, we have used a variety of bis(imine)-based tetradentate acyclic ligands as the structurally

non-rigid supporting ligand for the isolation of E(II) cationic species(E=Ge, Sn).[24] The flexibility at the ligand backbone has enabled geometric rearrangement thereby exposing

the frontier orbitals towards chemical reagents.[25] Very recently, we have also stabilized Sb(III) and Bi(III) mono- and di-cationic compounds and the Bi(III) tri-cationic (Figure 3) compound within the bis(alpha-iminopyridine) ligand (**L**) framework.[26]

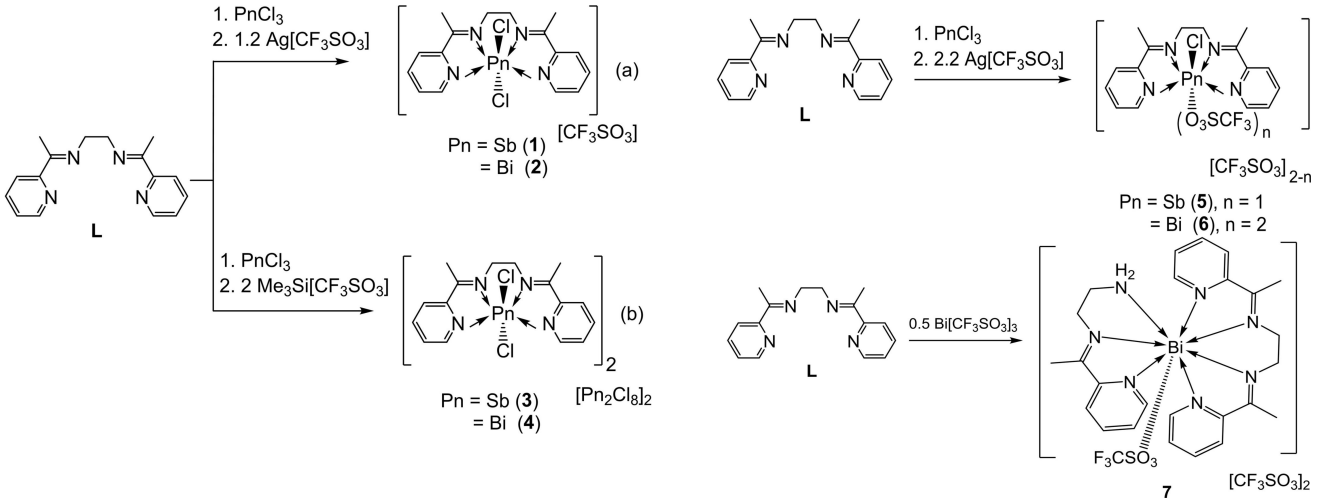

Figure 3. Antimony mono-cation (**1** & **3**) and di-cation (**5**); Bismuth mono-cation (**2** & **4**), di-cation (**6**) and tri-cation (**7**) stabilized with ligand **L**.

Herein, we have explored the bond lability of the tetra-cationic single bonded antimony and bismuth dimers **[1]$_2$** and **[2]$_2$**. Both the dimers undergo homolytic cleavage of their single bonds in the solution state giving rise to the monomer radicals, which have been characterized by EPR spectroscopy and absorption studies. Further, reactivity study done with the dimers **[1]$_2$** prove the lability of the sigma bond. Computational studies have been performed for a comprehensive understanding of the electronic features of **[1]$_2$** and **[2]$_2$.**

.

Chapter 2: Materials and Methods

Experimental Procedures

General Procedures:

All manipulations were carried out under a protective atmosphere of argon applying standard Schlenk techniques or in a dry box. Acetonitrile was stirred and refluxed over calcium hydride and kept over 3 Å molecular sieves. All solvents were distilled and stored under argon and degassed prior to use. Tetrahydrofuran was refluxed over sodium/benzophenone. CD_3CN ampoules were purchased from Sigma Aldrich and used as it is. All chemicals were used as purchased. ^{1}H and $^{13}C\{^{1}H\}$ NMR spectra were referenced to external $SiMe_4$ using the residual signals of the deuterated solvent (^{1}H) or the solvent itself ($^{13}C\{^{1}H\}$). ^{19}F and ^{77}Se were referenced to external $C_6H_5CF_3$ (TFT) and $SeMe_2$ (plus 5 % C_6D_6). NMR spectra were recorded on Bruker AVANCE III HD ASCEND 9.4 Tesla/400 MHz and Bruker AVANCE III HD ASCEND 14.1 Tesla/600 MHz NMR spectrometers. Solution phase UV/Vis spectra were acquired from SHIMADZU UV-1900 and UV-3600 plus UV-VIS-NIR spectrophotometer using quartz cells with a path length of 1 cm. Single crystal data were collected on both Bruker SMART APEX four-circle diffractometer equipped with a Bruker APEX-II CCD diffractometers using Mo Kα radiation (0.71073 Å).

Synthesis of ($[L(Sb^{2+})](OTf)_2)_2$ ($[1]_2$): Trimethylsilyltrifluoromethane sulfonate (TMSOTf) (0.35 mL, 1.86 mmol) was added to a mixture of $SbCl_3$ (0.14 g, 0.62 mmol) and **L** (0.16 g, 0.62 mmol) taken in 10 mL acetonitrile solvent and stirred for 5 minutes. To this resultant solution, 1.0 M solution of lithium borohydride in THF (0.62 mL, 0.62 mmol) was added and stirred for overnight. Product in the solution was collected through filtration and all the volatiles were evaporated to get a crude red solid. Orange single crystals of **$[1]_2$** was obtained from acetonitrile medium maintained at room temperature in 76 % yield (0.32 g).

^{1}H NMR (400 MHz, CD_3CN, 298 K, 2.91 mM) δ 9.28-9.26 (m, 2H, o-Pyr-H); 8.45-8.36 (m, 4H, m-Pyr-H); 8.02 (ddd, J = 7.0, 5.1, 1.7, 2H, p-Pyr-H); 4.41-4.24 (m, 4H, -CH_2-CH_2−); 2.85 (s, 6H, -CH_3) ppm.

$^{13}C\{^{1}H\}$ NMR (101 MHz, CD_3CN, 298 K, 32.78 mM) δ 176.76 (C–CH3); 176.22 (C–CH_3); 148.67 (Pyr-C_i); 148.56 (Pyr-C_i); 148.08 (Pyr-C_o); 147.32 (Pyr-C_o); 142.65 (Pyr-C_p); 142.44 (Pyr-C_p); 130.12 (Pyr-C_m); 130.08 (Pyr-C_m); 127.85 (Pyr-C_m); 127.81 (Pyr-C_m); 121.35 (q, J = 320 Hz, CF_3SO_3); 49.94 (−CH_2-CH_2−); 49.67 (−CH_2-CH_2−); 18.93 (−CH_3); 18.89 (-CH_3) ppm.

$^{19}F\{^{1}H\}$ NMR (377 MHz, CD3CN, 298 K, 32.78 mM) δ -79.36 (s) ppm.

Synthesis of ([L(Bi^{2+})](OTf)$_2$)$_2$ ([2]$_2$): Trimethylsilyltrifluoromethane sulfonate (TMSOTf) (0.20 mL, 1.14 mmol) was added to a mixture of $BiCl_3$ (0.12 g, 0.38 mmol) and **L** (0.10 g, 0.38 mmol) taken in 10 mL acetonitrile solvent and stirred for 5 minutes. To this resultant solution, 1.0 M solution of lithium borohydride in THF (0.38 mL, 0.38 mmol) was added and stirred for overnight. Product in the solution was collected through filtration and all the volatiles were evaporated to get a crude red solid. Orange single crystals of **[2]$_2$** was obtained from acetonitrile medium maintained at room temperature in 71% yield (0.21 g).

^{1}H NMR (400 MHz, CD_3CN, 298 K) δ 8.74 (dd, J = 5.0, 0.9, 2H, o-Pyr-H); 8.10 (td, J = 7.9, 1.6, 2H, m-Pyr-H); 7.93 (d, J = 8.0, 2H, m-Pyr-H); 7.78 (ddd, J = 7.6, 5.1, 0.9, 2H, p-Pyr-H); 4.82-4.69 (m, 2H, -CH_2-CH_2−); 4.63-4.49 (m, 2H, -CH_2-CH_2−); 2.80 (s, 6H, -CH_3) ppm.

^{13}C{^{1}H} NMR (101 MHz, CD_3CN, 298 K) δ 178.72 (C–CH_3); 151.21 (Pyr-C_i); 149.96 (Pyr-C_o); 142.49 (Pyr-C_p); 129.56 (Pyr-C_m); 128.72 (Pyr-C_m); 121.41 (q, J = 320 Hz, CF_3SO_3); 55.02 (−CH_2-CH_2−); 20.76 (−CH_3) ppm.

^{19}F{^{1}H} NMR (377 MHz, CD3CN, 298 K) δ -79.12 (s) ppm.

Synthesis of [L(Sb-SPh)](OTf)$_2$ (3): Diphenyl disulfide (0.006 g, 29 µmol) was added to solution of **[1]$_2$** (0.04 g, 29 µmol) in 10 mL acetonitrile and stirred at ambient temperature for 4 hours. Pale greenish-yellow single crystals of **3** was obtained from acetonitrile medium maintained at room temperature in 73% yield (0.03 g).

^{1}H NMR (400 MHz, CD_3CN, 298 K) δ 9.24 (ddd, *J* = 5.1, 1.5, 0.7, 2H, *o*-Pyr-H); 8.30 (td, *J* = 7.9, 1.6, 2H, *m*-Pyr-H); 8.18 (d, *J* = 8.0, 2H, *m*-Pyr-H); 7.98 (ddd, *J*=7.7, 5.1, 1.1, 2H, *p*-Pyr-H); 7.11-7.04 (m, 1H, *p*-SPh-H); 6.97-6.90 (m, 2H, o-SPh-H); 6.85-6.81 (m, 2H, m-SPh-H); 4.42 (s, 4H, -CH_2-CH_2−); 2.72 (s, 6H, -CH_3) ppm.

^{13}C{^{1}H} NMR (101 MHz, CD_3CN, 298 K) δ 176.37 (C–CH_3); 148.52 (Pyr-C_i); 147.16 (Pyr-C_o); 142.58 (Pyr-C_p); 136.37 (SPh-C_i); 130.81 (SPh-C_p); 130.39 (SPh-C_o); 129.59 (Pyr-C_m); 129.30 (SPh-C_m); 127.80 (Pyr-C_m); 121.58 (q, J =322 Hz, CF_3SO_3); 49.86 (−CH_2-CH_2−); 19.24 (−CH_3) ppm.

^{19}F{^{1}H} NMR (377 MHz, CD_3CN, 298 K) δ -79.33 (s) ppm.

Synthesis of [L(Sb-SePh)](OTf)$_2$ (4): Diphenyl diselenide (0.009 g, 29 µmol) was added to solution of **[1]$_2$** (0.04 g, 29 µmol) in 10 mL acetonitrile and stirred at ambient temperature for 4 hours. Pale greenish-yellow single crystals of **4** was obtained from acetonitrile medium maintained at room temperature in 79% yield (0.04 g).

^{1}H NMR (400 MHz, CD_3CN, 298 K) δ 9.28-9.22 (m, 2H, *o*-Pyr-H); 8.28 (td, *J* = 7.9, 1.6, 2H, *m*-Pyr-H); 8.17 (d, *J* = 8.0, 2H, *m*-Pyr-H); 7.97 (ddd, *J*=7.7, 5.1, 1.1, 2H, *p*-Pyr-H); 7.15-7.08 (m, 1H, *p*-SePh-H); 6.97-6.88 (m, 4H, o-SePh-H and m-SePh-H); 4.43 (s, 4H, -CH_2-CH_2−); 2.70 (s, 6H, -CH_3) ppm.

$^{13}C\{^1H\}$ NMR (101 MHz, CD_3CN, 298 K) δ 176.15 (C–CH_3); 148.62 (Pyr-C_i); 147.42 (Pyr-C_o); 142.71 (Pyr-C_p); 137.57 (SePh-C_i); 130.44 (SePh-C_p); 129.93 (SePh-C_o); 129.71 (Pyr-C_m); 128.05 (SePh-C_m); 126.78 (Pyr-C_m); 121.76 (q, J = 322 Hz, CF_3SO_3); 50.15 (−CH_2-CH_2−); 19.46 (−CH_3) ppm.

$^{19}F\{^1H\}$ NMR (377 MHz, CD_3CN, 298 K) δ -79.28 (s) ppm.

Synthesis of $[L_2(Sb^{2+})_2C_6H_4O_2][OTf]_4$(5): p-Benzoquinone (0.003 g, 29 µmol) was added to solution of **[1]$_2$** (0.04 g, 29 µmol) in 10 mL acetonitrile and was stirred at ambient temperature for 4 hours. Orange single crystals of **5** was obtained from acetonitrile medium maintained at room temperature in 81% yield (0.03 g).

^1H NMR (400 MHz, CD_3CN, 298 K) δ 9.29-9.26 (m, 1H, *o*-Pyr-H); 9.25-9.22 (m, 1H, *o*-Pyr-H); 9.07-9.01 (m, 2H, *o*-Pyr-H); 8.44-8.36 (m, 2H, *m*-Pyr-H); 8.35-8.30 (m, 1H, *m*-Pyr-H); 8.29-8.26 (m, 1H, *m*-Pyr-H); 8.14 (td, *J*=7.9, 1.4, 1.1, 2H, *p*-Pyr-H); 8.04-7.95 (m, 4H, *m*-Pyr-H); 7.85-7.78 (m, 2H, *p*-Pyr-H); 6.65 (s, 1H, $C_6H_4O_2$-H); 6.36 (s, 1H, $C_6H_4O_2$-H); 6.35-6.30 (m, 1H, $C_6H_4O_2$-H); 6.16-6.11 (m, 1H, $C_6H_4O_2$-H); 4.64-4.53 (m, 2H, -CH_2-CH_2−); 4.44-4.24 (m, 6H, -CH_2-CH_2−); 2.85 (s, 3H, -CH_3) ppm; 2.77 (s, 3H, -CH_3) ppm; 2.64 (s, 6H, -CH_3) ppm.

$^{13}C\{^1H\}$ NMR (151 MHz, CD_3CN, 298 K) δ 177.03 (C–CH_3); 176.95 (C–CH_3); 175.62 (C–CH_3); 151.91 (-$C_6H_4O_2$, -O-C); 151.82 (-$C_6H_4O_2$, -O-C); 148.91 (Pyr-C_i); 148.40 (Pyr-C_i); 148.28 (Pyr-C_i); 147.98 (Pyr-C_i); 146.96 (Pyr-C_o); 146.90 (Pyr-C_o); 146.71 (Pyr-C_o); 142.09 (Pyr-C_p); 141.93 (Pyr-C_p); 129.90 (Pyr-C_m); 129.75 (Pyr-C_m); 129.52 (Pyr-C_m); 127.23 (Pyr-C_m); 127.07 (Pyr-C_m); 120.4 (q, J=323.2 Hz, CF_3SO_3); 115.77 (-$C_6H_4O_2$, -H-C); 115.67 (-$C_6H_4O_2$, -H-C); 115.02 (-$C_6H_4O_2$, -H-C); 114.93 (-$C_6H_4O_2$, -H-C); 49.37 (−CH_2-CH_2−); 49.18 (−CH_2-CH_2−); 18.44 (−CH_3); 18.38 (−CH_3) ppm.

$^{19}F\{^1H\}$ NMR (377 MHz, CD_3CN, 298 K) δ -79.33 (s).

Synthesis of $[L_2(Sb^{2+})_2O](OTf)_4$ (6): Method A: In a Schlenk flask **[1]$_2$** (0.04 g, 29 µmol) was dissolved in 15 mL acetonitrile and subsequently exposed to air. The solution was then stirred at ambient temperature for 5 hours. Product in the solution was collected through filtration and concentrated. Colorless single crystals of **6** was obtained from acetonitrile medium maintained at -30^{o}C in 59% yield (0.025 g).

Method B: TEMPO (0.004 g, 29 µmol) was added to solution of **[1]$_2$** (0.04 g, 29 µmol) in 10 mL acetonitrile and was stirred at ambient temperature for overnight. Then the reaction mixture was concentrated. Colorless single crystals of **6** was obtained from acetonitrile medium maintained at -30^{o}C in 53% yield (0.02 g).

^1H NMR (400 MHz, CD_3CN, 298 K) δ 9.03 (dt, *J* = 5.2, 1.2, 2H, *o*-Pyr-H); 8.26-8.23 (m, 4H, *m*-Pyr-H); 7.82-7.78 (m, 2H, *p*-Pyr-H); 4.36-4.18 (m, 4H, -CH_2-CH_2−); 2.68 (s, 6H, -CH_3) ppm.

$^{13}C\{^1H\}$ NMR (101 MHz, CD_3CN, 298 K) δ 168.81 (C–CH_3); 150.01 (Pyr-C_i); 148.51 (Pyr-C_o); 142.28 (Pyr-C_p); 129.05 (Pyr-C_m); 126.88 (Pyr-C_m); 121.3 (q, J=322 Hz, CF_3SO_3); 50.22 (−CH_2-CH_2−); 17.20 (−CH_3) ppm.

$^{19}F\{^1H\}$ NMR (377 MHz, CD_3CN, 298 K) δ -79.32 (s) ppm.

Chapter 3: Results and Discussion

Syntheses and Basic Spectroscopic Characterization

The ligand **L** was synthesized via Schiff base condensation of 2-acetylpyridine with ethylenediamine in a 2:1 molar ratio following the literature procedure. [27] $PnCl_3$ (Pn = Sb and Bi) and **L** were taken in 1:1 ratio followed by the addition of three equivalents of trimethylsilyltrifluoromethane sulfonate. Addition of lithium borohydride to the resulting mixture gave the reduced dimeric products $[L(Sb^{2+})][(OTf)_2]_2$ **[1]$_2$** and $[L(Bi^{2+})][(OTf)_2]_2$ **[2]$_2$** respectively in moderate yields (Scheme 1). Both the compounds were characterized by multi-nuclear NMR spectroscopy and absorption studies in the solution-state and single crystal X-ray diffraction technique in the solid-state.

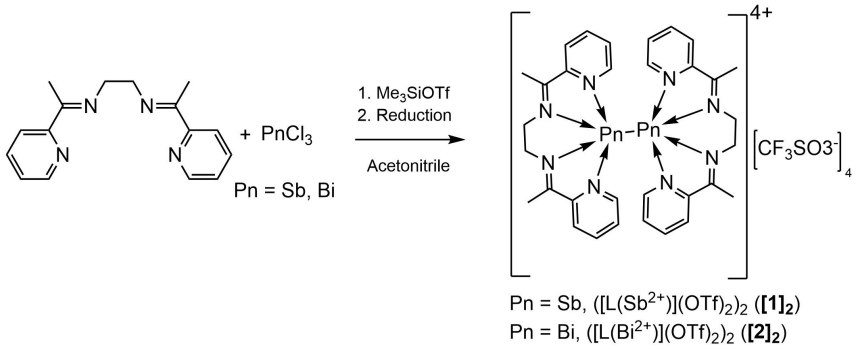

Scheme 1. Syntheses of compounds **[1]$_2$** and **[2]$_2$** in a acetonitrile medium.

Compound **[1]$_2$** crystallizes in monoclinic $P2_1/c$ space group containing $([L(Sb^{2+})])_2$ tetracation, three non-coordinating triflate anion and a weakly coordinating triflate anion in the asymmetric unit (Figure 4a and Table 1). In the molecular structure of the cationic part in **[1]$_2$**, two singly-bonded Sb centers are present. Both Sb centers are tetra-coordinated by the two imino (N_{im}) (N2, N3 & N6, N7) and two pyridine (N_{py}) (N1, N4 & N5, N8) nitrogens forming a distorted planar geometry (torsional angle N1-N2-N3-N4 = -11.0(9)° and N5-N6-N7-N8 = -7.0(9)°) around it. To minimize the steric repulsion, two ligands prefer *anti*-position in the solid state. The Sb-Sb bond length of 3.0273(18) Å observed in **[1]$_2$** is considerably longer than that of other reported neutral distibanes (non-bulky systems) (2.835(1) - 2.9194(6) Å).[17] However, the Sb-Sb bond distance in **[1]$_2$** closely resembles highly bulky distibane system present in **[III]$_2$** and **II** (-R = Dmp) which show radical character in the solution state by homolytically breaking the Sb-Sb bond. In contrast to steric bulk present in **[III]$_2$** and **II**, our hypothesis supported by Natural Bond Orbital (NBO) analysis (NBO charges on each Sb = +1.17), suggests that coulombic repulsion between the two cationic antimony centers contribute to the bond's labile nature. Notably, only one

triflate anion is very loosely bound to the Sb1 center in the axial position (Sb1-O1 = 3.44(2) Å), exceeding the sum of covalent radii ($\Sigma_{r,cov}$(Sb-O) = 2.03 Å),[20] however falls within the sum of van der Waal's radii ($\Sigma_{r,vdW}$(Sb-O) = 3.58 Å).[20] The other three triflate anions are entirely devoid of any interaction with the Sb center, lying outside the van der Waal's radii. The Sb-N_{im} bond lengths are shorter (Sb1-N2 = 2.273(15) and Sb1-N3 = 2.255(12) Å; Sb2-N6 = 2.260(15) and Sb2-N7 = 2.262(13) Å) compared to the Sb-N_{py} distances (Sb1-N1 = 2.510(12) and Sb1-N4= 2.448(13) Å; Sb2-N5 = 2.489(12) and Sb2-N8 = 2.451(14) Å) in **[1]$_2$** which closely resemble with Sb-N bond distance present in L stabilized antimony di-cation[26].

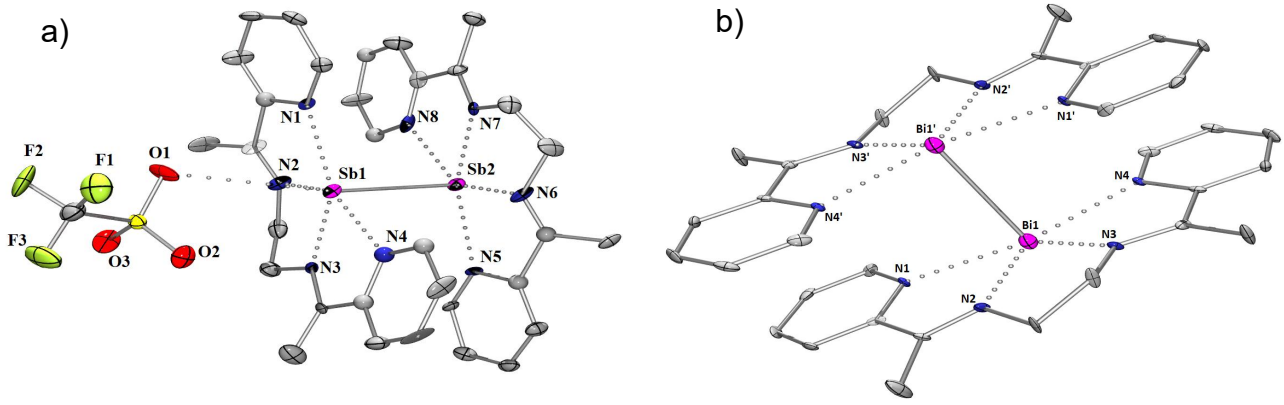

Figure 4. Molecular structure of the cationic parts of **[1]$_2$**(a) and **[2]$_2$**(b) in the solid state (thermal ellipsoids at 30%, H atoms and counter anions are omitted for clarity). Selected bond lengths [Å] and angle [°]: a) Sb1-N1 = 2.510(12), Sb1-N2 = 2.273(15), Sb1-N3 = 2.255(12), Sb1-N4= 2.448(13), Sb2-N5 = 2.489(12), Sb2-N6 = 2.260(15), Sb2-N7 = 2.262(13), Sb2-N8 = 2.451(14), Sb1-Sb2 = 3.0273(18); b) Bi1-N1 = Bi1'-N1' = 2.536(5), Bi1-N2 = Bi1'-N2' = 2.365(5), Bi1-N3 = Bi1'-N3' = 2.381(6), Bi1-N4 = Bi1'-N4' = 2.576(5), Bi1-Bi1' = 3.1403(7). (Note: weakly coordinating counter anions have been omitted for clarity in case of **[2]$_2$**. Please see Figure S22 for the complete structure)

Compound **[2]$_2$** crystallizes in the triclinic P-1 space group (Figure 4b, Table 2). Only half of the unit is present in the asymmetric unit and the other half is generated by the inversion operation. The asymmetric unit contains ([L(Bi^{2+})]) di-cation (monomer) and corresponding four weakly coordinating triflate anions, resulting in both bismuth centers hepta-coordinated in the dimeric structure (Figure S22). The large-sized Bi atoms have led to this hepta-coordination. The covalent radii for Bi-O is $\Sigma_{r,cov}$(Bi-O) = 2.14 Å,[20] while van der Waal's radii is ($\Sigma_{r,vdW}$(Bi-O) = 3.59 Å).[20] All the Bi-O (triflate) bond distances are longer than the Bi-O covalent radii but fall within the range of van der Waal's radii,[20] with Bi1-O2 = Bi1'-O2' = 2.774(4), Bi1-O4 = Bi1'-O4' = 3.025(6) Å. The Bi-Bi distance of 3.1403(7) Å is longer compared to Bi-Bi bond lengths of reported dibismuthanes (non-bulky systems) (2.9902(5)–3.087(3) Å).[17] However, the Bi-Bi bond distance in **[2]$_2$** is like highly bulky dibismuthane system present in **[IV]$_2$**, known for its radical character in the solution state

due to homolytic cleavage of the Bi-Bi bond. Like **[1]$_2$**, this elongated bond distance is attributed to coulombic repulsion between the two cationic bismuth centers (NBO charges on each Bi = + 1.2). The larger size of Bi atom leads to longer Bi-N_{im} (Bi1-N2 = Bi1'-N2' = 2.365(5) and Bi1-N3 = Bi1'-N3' = 2.381(6)) and Bi-Npy (Bi1-N1 = Bi1'-N1' = 2.536(5) and Bi1-N4 = Bi1'-N4' = 2.576(5)) bond lengths compared to **[1]$_2$**.

Interestingly, **[1]$_2$** shows a concentration-dependent colour change in acetonitrile solvent. At very high concentrations, it maintains a reddish-orange colour (10 mM or above), while extreme dilution (0.15 mM or below) causes the colour to shift to dark blue, with an intermediate green colour observed at moderate concentrations (0.3 mM to 4 mM). These observations are consistent with UV-Vis spectroscopy data (Figure 5a) of **[1]$_2$** in acetonitrile solvent, which reveal characteristic absorption peaks corresponding to each observed colours. The absorbance spectrum of a highly diluted solution (0.146 mM & 0.226 mM, Figure 5a) of **[1]$_2$** in acetonitrile shows a λ_{max} at 639 nm and a hump at 693 nm, indicative of a blue-coloured solution. For an intermediate concentration (0.299 mM to 0.73 mM), a green-coloured solution emerges with two new peaks at 559 nm and 408 nm alongside peaks at 639 nm and 693 nm, corresponding to reddish-orange colour. Notably, this suggests that green solution is a mixture of the blue species (639 nm & 693 nm) and the reddish-orange species (408 nm & 559 nm). Based on these observations and highly elongated Sb-Sb bond observed in **[1]$_2$** in the solid state, we hypothesize that **[1]$_2$** exists in a monomer-dimer equilibrium in acetonitrile. The monomer, a Sb-centered radical di-cation ($L(Sb^{2+})(OTf)_2$) (**[1]**·), forms after the homolytic cleavage of the Sb-Sb bond in the acetonitrile solution, displaying an intense dark blue colour (639 nm & 693 nm), while the dimer (**[1]$_2$**) exhibits a reddish-orange colour (408 nm & 559 nm). It is noteworthy that the blue solution corresponding to the monomer radical is stable for only 20 - 25 minutes, even under inert glove box conditions at -30°C. This limited stability has deterred us from measuring the monomer-dimer equilibrium constant and drawing conclusions regarding the relationship between the intensity of the monomer peak and the concentration of **[1]$_2$** in the acetonitrile solvent.

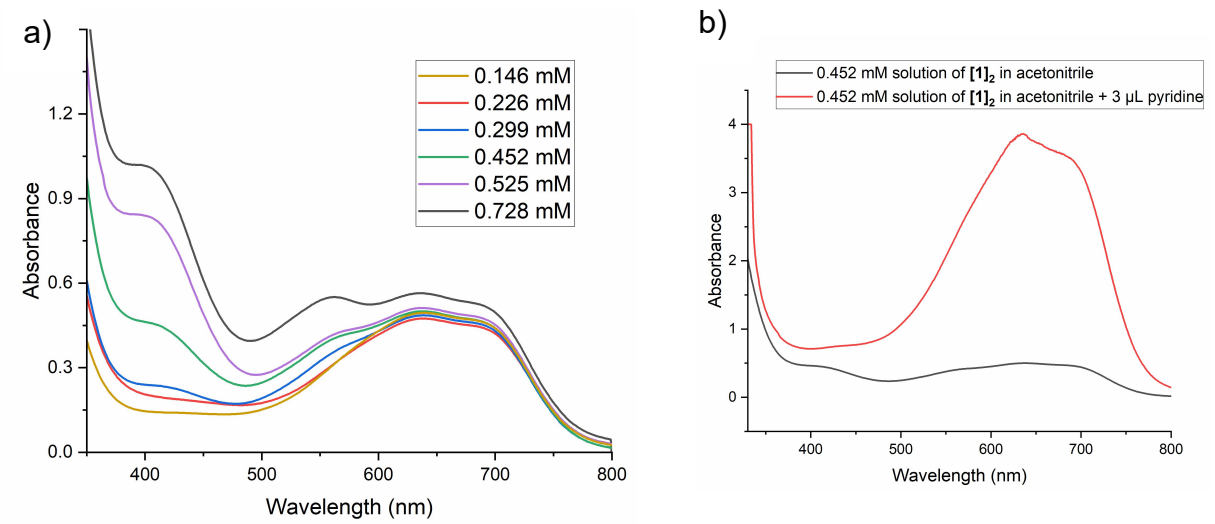

Figure 5. (a) UV-Vis spectra of a solution of **[1]$_2$** in acetonitrile in six different concentrations - 0.728 mM (black), 0.525 mM (purple), 0.452 mM (green), 0.299 mM (blue), 0.226 mM (red) and 0.146 mM (yellow); (b) UV-Vis spectra of a 0.452 mM solution of **[1]$_2$** in acetonitrile (black) and 0.452 mM solution of **[1]$_2$** in acetonitrile + 3 µL pyridine (red).

Another interesting observation is made when a single drop of pyridine is added to concentrated solutions (0.452 mM or higher) of **[1]$_2$** in acetonitrile solvent. This addition results in a dark blue solution with the same λ_{max} at 639 nm and a hump at 693 nm as observed in the highly diluted solution (0.146 mM) of **[1]$_2$** in acetonitrile (Figure 5b). This confirms that the addition of a very small amount of pyridine shifts the monomer-dimer equilibrium towards the monomer radical (**[1]**·).

The formation of compounds **[1]$_2$** and **[2]$_2$** was characterized using multi-nuclear NMR spectroscopy in CD_3CN solvent (Figure S1–S8). The ^{1}H NMR spectra of **[1]$_2$** exhibited a concentration-dependent behavior. At low concentrations (2.91 mM) (Figure S1), only one set of peaks was observed, attributed to the monomer (**[1]**·), as there is a lesser amount of dimer present at low concentration. Conversely, at higher concentrations (32.78 mM) (Figure S1–S2), where both dimer and monomer are present, two sets of peaks were observed: one attributed to the monomer, consistent with the low concentration spectrum, and another new set attributed to the dimer. It is noteworthy that all signals observed in CD_3CN solvent were well-defined (no broad signals), which can be explained by their low Mulliken spin density in the ligand backbone (Figure 6).[32] Similarly, the $^{13}C\{^1H\}$ spectrum of **[1]$_2$** at high concentration (Figure S4) also exhibited two different sets of peaks attributed to the monomer and dimer. In contrast, **[2]$_2$** displayed only one set of peaks in both the ^{1}H and $^{13}C\{^1H\}$ NMR spectra (Figures S6-S7) at high concentration, likely due to the presence of only the monomer in the solution state. The $^{19}F\{^1H\}$ resonances of **[1]$_2$** and

[2]$_2$ was observed at around -79 ppm (Figures S5 and S8), indicative of dissociated triflate anions, consistent with earlier literature reports.[26] The formation of the radical (**[1]**·) in the solution state is further supported by EPR spectroscopy. The EPR of **[1]$_2$** displayed a broad signal (Figure 7), similar to EPR spectra observed for **[III]**· and the distibene anion radical reported by Tokitoh and Sasamori.[28]

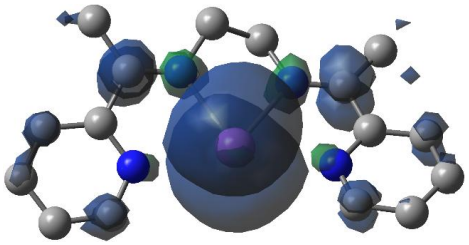

Figure 6. Spin density of the monomer **[1]**·

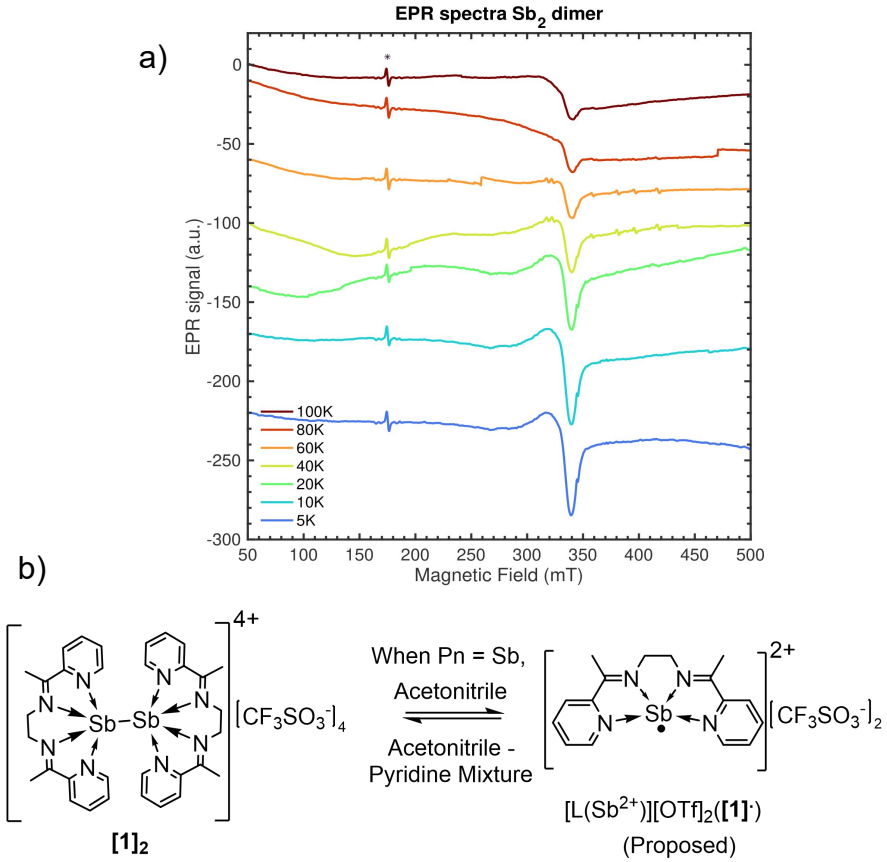

Figure 7: a) EPR spectrum of **[1]$_2$** in acetonitrile measured at different temperatures (100K - 5K) (top); b) Scheme of the formation of **[1]**· from **[1]$_2$** and the proposed structure of **[1]**· (bottom).

Reactivity Studies

Absorption, NMR, and EPR spectroscopy studies confirm the formation of radical species from **[1]$_2$** in the solution state, although they do not ascertain an antimony-centered radical. To determine the site of radical formation and reactivity, reactivity studies of **[1]$_2$** with O_2, E_2Ph_2 (E = S, Se), 1,4-benzoquinone, and TEMPO were conducted (Scheme 2 & 3). Based on the previous observations, it is hypothesized that homolysis of the Sb-Sb bond occurs in the acetonitrile solution, generating an **L**-stabilized Sb(II) radical dication (**[1]**$^{\cdot}$) that will participate in the reaction. Reactivity studies indicate that the reactions indeed occur at the Sb center, supporting our hypothesis.

Distibanes are conventionally known to react with diorgano dichalcogenides, resulting in the cleavage of the two element-element bonds and the formation of an antimony-chalcogen bond.[29] However, here, **[1]$_2$** follows a radical quenching pathway, generating a radical (**[1]**$^{\cdot}$) in the solution state that cleaves the E−E bond present in PhE−EPh and forms an Sb-EPh bond. **[1]$_2$** and diphenyl dichalcogenides PhE−EPh (E=S, Se) readily react at room temperature in acetonitrile in 1:1 ratio (Scheme 2). These reactions lead to the formation of two **L**-stabilized Sb-EPh di-cations, [L.Sb-EPh](OTf)$_2$ (**3** when E = S & **4** when E = Se). To the best of our knowledge, **3** and **4** represent the first reported antimony-chalcogenide cations. Light greenish yellow-colored single crystals of both **3** and **4** suitable for X-ray diffraction have been obtained in 73% and 79% yields respectively. Compounds **3** and **4** were characterized by multinuclear NMR studies in CD_3CN (Figures S9-S15). ^1H and $^{13}C\{^1H\}$ spectra exhibit an obvious downfield shift compared to the free ligand **L,**[25a] attributed to the presence of di-cationic charges in **3** and **4**.

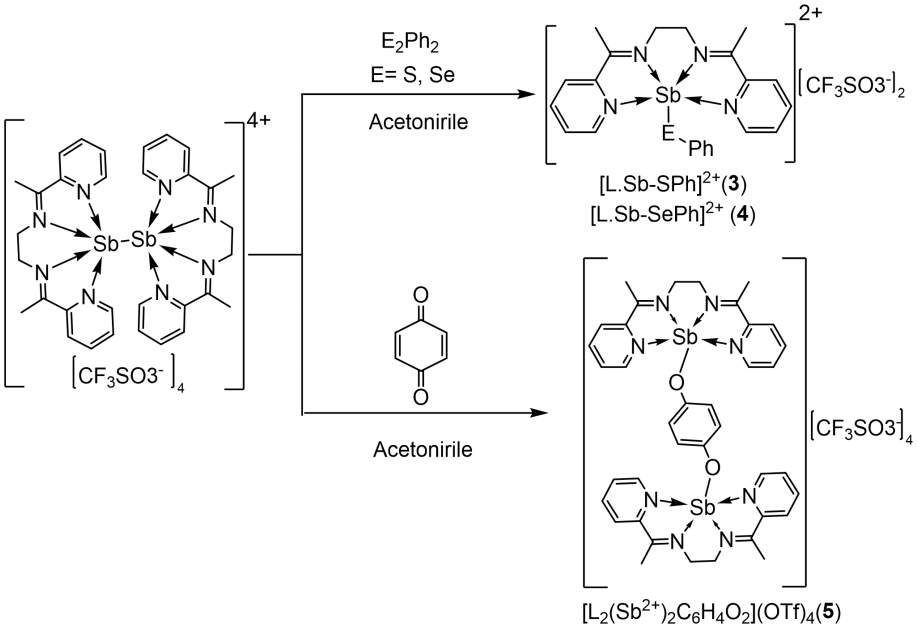

Scheme 2. Synthesis of **3**-**5** in the acetonitrile medium.

Compound **3** crystallizes in the triclinic P-1 space group, with the asymmetric unit containing the [LSb-SPh(OTf)] cation and the corresponding [OTf] anion (Figure 8a, Table 3), forming a formally di-cationic species. One triflate anion is weakly coordinating to the Sb center (Sb1-O1 = 3.192(3) Å), with a length longer than the sum of Sb-O covalent radii, but falling within the sum of Sb-O van der Waals radii. The other triflate anion remains completely uninvolved with the Sb center. However, solution-state $^{19}F\{^{1}H\}$ NMR study (Figure S11) shows peak at δ = -79.3 ppm for both the triflate anions present, indicating dissociated triflate anions in the solution state, unlike in its solid-state structure. Compound **3** adopts a distorted octahedral geometry, with the four nitrogen centers lying in the distorted plane and the -SPh and triflate anion occupy the axial sites. The Sb-N_{im} bond lengths are Sb1-N2 = 2.2572(19) and Sb1-N3 = 2.291(2) Å while Sb-N_{py} bonds are Sb1-N1 = 2.399(2) and Sb1-N4= 2.516(2) Å, closely resembling the Sb-N bond lengths in **[1]$_2$**. The Sb1-S1 bond, nearly *trans* to O1(OTf), exhibits a length of 2.4473(6) Å. The only reported crystal structure featuring Sb-organosulphide[30] bond has an Sb-S bond length of 2.5218(12) Å, longer than the Sb-S bond length observed in **3**. The comparatively shorter bond length in **3** might be attributed to sulphur's lone pair electron to antimony vacant p orbital back donation.

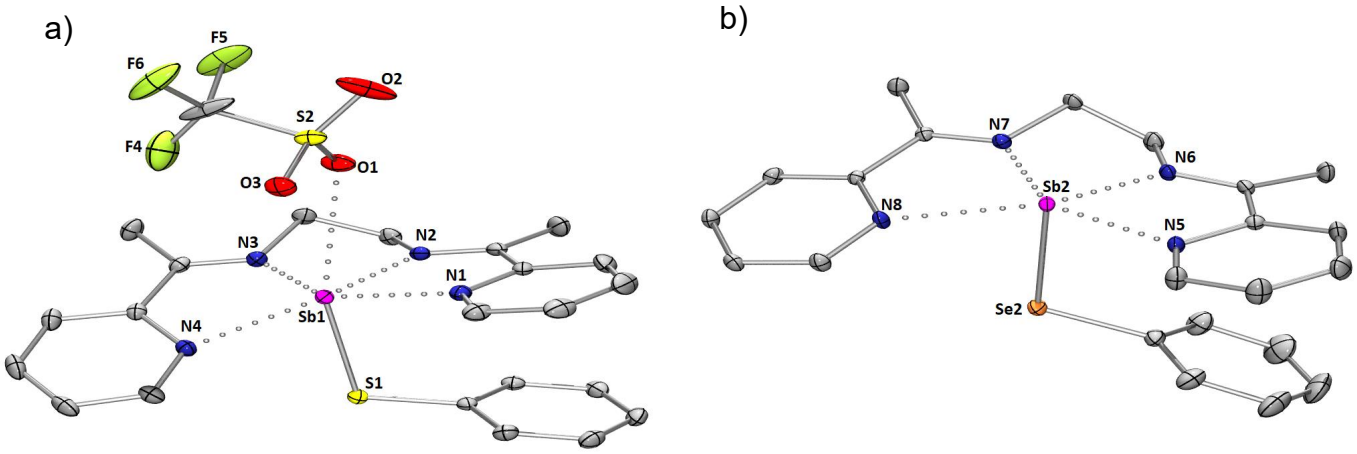

Figure 8. Molecular structure of the cationic parts of **3**(a) and **4**(b) in the solid state (thermal ellipsoids at 30%, H atoms and counter anions are omitted for clarity). Selected bond lengths [Å] and angle [º]: a) Sb1-N1 = 2.399(2), Sb1-N2 = 2.2572(19), Sb1-N3 = 2.291(2) Å, Sb1-N4 = 2.516(2), Sb1-S1 = 2.4473(6); b) Sb2-N5 = 2.358(3), Sb2-N6 = 2.231(2), Sb2-N7 = 2.345(3), Sb2-N8 = 2.635(3), Sb2-Se2 = 2.5437(4).

Compound **4** crystallizes in the triclinic P-1 space group. The crystal lattice of **4** comprises of one [LSb-SePh(OTf)] cation, one [LSb-SePh] di-cation and corresponding three triflate counter anions present within the asymmetric unit (Figure 8b, Table 4). In the solution state, all triflate anions exhibit only one peak in the $^{19}F\{^{1}H\}$ NMR (Figure S14) at δ = -79.28

ppm, indicating their non-coordinating behaviour in the solution state. Additionally, the ^{77}Se NMR spectrum displays only one peak at δ = 270.46 ppm (Figure S15), suggesting that the [LSb-SePh(OTf)] cation dissociates the triflate anion in the solution state and behaves similarly to the [LSb-SePh] dication. Both cation units present in the asymmetric unit are structurally similar, except for one cationic part ([LSb-SePh(OTf)] cation) (Figure S23), where the Sb centre is weakly coordinated by one triflate (Sb1-O4 = 2.858(2) Å). This adopts a distorted pentagonal pyramidal geometry in the solid state, with four nitrogen centers from **L** and one oxygen atom from triflate anion lying in the distorted plane, while the -SePh occupies the axial sites. The other cationic part (Figure 8b) is free from any triflate coordination and adopts a distorted square pyramidal geometry. The Sb-N_{im} bond lengths are Sb2-N6 = 2.231(2) and Sb2-N7 = 2.345(3) Å while Sb-N_{py} bonds are Sb2-N5 = 2.358(3) and Sb2-N8 = 2.635(3) Å, closely resembling the Sb-N bond lengths in **3**. Compound **4** exhibits a Sb2-Se2 bond length of 2.5437(4) Å. To the best of our knowledge, this is the first reported crystal structure featuring an Sb-organoselenide bond. The highly downfield shifted ^{77}Se NMR peak, compared to the Bi-organoselenide bond (neutral species, δ = 175.70 ppm) reported by Lichtenberg *et al.,*[31] serves as an indicator of selenium's lone pair electron to antimony vacant p orbital back donation.

The room temperature reaction between **[1]$_2$** and 1,4-benzoquinone in 1:1 ratio in acetonitrile resulted in the formation of compound **5** (Scheme 2). Orange single crystals of **5** suitable for X-ray diffraction were obtained in 81% yield. This reaction also follows radical quenching pathway. Multinuclear NMR studies (^{1}H, ^{13}C{^{1}H}, ^{19}F{^{1}H}) in CD_3CN (Figures S16–S18) confirmed the formation of **5**. Like **3** and **4**, the ^{1}H and ^{13}C{^{1}H} NMR spectrum of **5** exhibited downfield shifted compared to **L**. The UV-Visible spectrum of **5** could not be measured due to its limited stability in the solution state and its high sensitivity to both moisture and air.

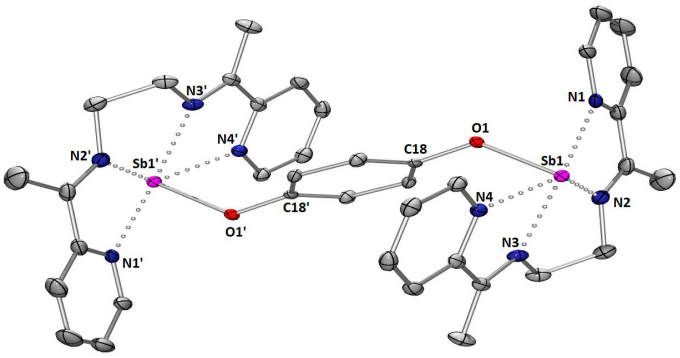

Figure 9. Molecular structure of the cationic part of **5** in the solid state (thermal ellipsoids at 30%, H atoms and counter anions are omitted for clarity). Selected bond lengths [Å] and angle [º]: Sb1-N1 = Sb1'-N1' =

2.460(4), Sb1-N2 = Sb1'-N2' = 2.267(4), Sb1-N3 = Sb1'-N3' = 2.293(4), Sb1-N4 = Sb1'-N4' = 2.497(4), Sb1-O1 = Sb1'-O1' = 1.965(3), C18-O1 = C18'-O1' = 1.378(5), C18-O1-Sb1 = C18'-O1'-Sb1' = 130.3(2).

Complex **5** crystallizes in the triclinic P-1 space group as determined from the X-ray diffraction data (Figure 9, Table 5). The asymmetric unit comprises only half of compound **5**, and the full molecule was generated by inversion operation. The fully grown structure consists benzene-1,4-bis(olate) ($[C_6H_4O_2]^{2-}$) bridged **L-**coordinated two antimony cation centres ($[L_2(Sb^{2+})_2C_6H_4O_2(OTf)_2]$ and corresponding two free triflate anions. One triflate anion is weakly coordinating to each Sb center, while the other two triflates remain uncoordinated. Due to significant disorder in the triflates coordinating to the Sb centers, they are omitted for clarity. However, in CD_3CN all triflates exhibit a peak at -79.33 ppm in the $^{19}F\{^1H\}$ NMR (Figure S18), indicating formally tetra-cationic compound **5** exhibits equivalent triflate anions in solution, contrary to its solid-state structure. Each Sb center adopts a distorted pentagonal pyramidal geometry in the solid state, with four nitrogen centers from **L** and one oxygen atom from a coordinating triflate anion lying in the distorted plane, while the oxygen atom from benzene-1,4-bis(olate) ($[C_6H_4O_2]^{2-}$) occupies the axial sites. From the crystal structure, it is evident that compound **5** lacks symmetry which is also reflected in the solution state (^1H and $^{13}C\{^1H\}$ NMR spectra of compound **5**). Although, tetraphenyl distibane is known to react with 1,4-benzoquinone[13e] to yield benzene-1,4-bis(olate) ($[C_6H_4O_2]^{2-}$) bridged two $Ph_2Sb(III)$ centers, no crystal structure of benzene-1,4-bis(olate) ($[C_6H_4O_2]^{2-}$) bridged two $R_2Sb(III)$ centers has been reported so far. The Sb(III) radical cation reported by Tan *et al.*[32] also shows exhibit reactivity with 1,4-benzoquinone, yielding benzene-1,4-bis(olate) bridged two $R_2Sb(V)$ mono-cations.

The reaction of distibanes with dioxygen typically results in the insertion of one oxygen atom into the antimony-antimony bond.[33] In some distibanes, it also leads to hexoxides $(R_2Sb)_4O_6$, and peroxo clusters, $(R_2SbO)_4(O_2)_2$.[33][34] Exposure of a solution of **[1]$_2$** in acetonitrile to air leads to the formation of **6** (Scheme 3a). The same compound **6** was obtained when **[1]$_2$** reacted with TEMPO in a 1:1 ratio (Scheme 3b). A similar oxo transfer reaction occurred with Sb(III) radical cation[32] in the presence of TEMPO. Colorless single crystals of **6**, suitable for X-ray diffraction were obtained in 59% and 53% yields. The formation of compounds **6** was characterized using multi-nuclear NMR spectroscopy in CD_3CN solvent (Figures S19-S21).

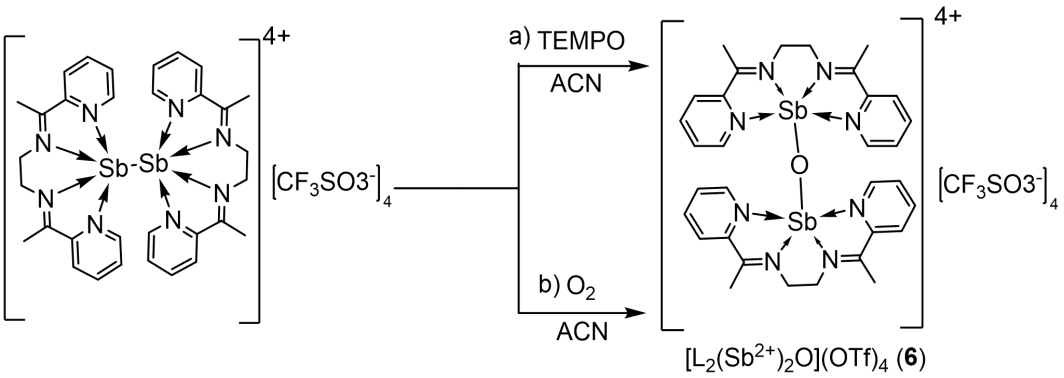

Scheme 3. Synthesis of **6** in the acetonitrile medium.

Compound **6** crystallizes in the monoclinic C2/c space group, with the asymmetric unit containing the $[L_2(Sb^{2+})_2O(OTf)_3]$ cation and the corresponding [OTf] anion (Figure 10, Table 6), forming a formally tetra-cationic species. The $[L_2(Sb^{2+})_2O(OTf)_3]$ cation unit comprises oxo-bridged two Sb(III) cationic centers, where one of the antimony centers is coordinated by two weakly coordinating triflate anions and the other one is coordinated by only one triflate anion. These coordination result in one antimony center adopting a distorted pentagonal bipyramidal geometry, while the other antimony center adopts a distorted pentagonal pyramidal geometry. However, in contrast to solid state, in the solution state (CD_3CN) all the triflate anions behave similarly as they all show a single peak in the $^{19}F\{^1H\}$ NMR (Figure S21) at -79.32 ppm. Due to presence of highly distorted defects of triflates, they are omitted for clarity. In the solid state, the two ligands are in the *anti*-position like **[1]$_2$**. Interestingly, all previously reported compounds comprising $R_2Sb(III)$-O-$Sb(III)R_2$ exhibit a bent Sb-O-Sb angle, with Sb-O-Sb bond angles ranging from 121.4(2) to 126.5(1)°.[33] However, to the best of our knowledge, this is the first reported linear oxo-bridged di-antimony tetra-cation, featuring an Sb-O-Sb bond angle of 177.0(4)°, which is attributed to strong back-donation from the oxygen lone pairs to the vacant p orbitals of the antimony centers. Consequently, the Sb-O bond lengths also become shorter compared to previously reported $R_2Sb(III)$-O-$Sb(III)R_2$ molecules,[33] with Sb-O bond lengths of Sb1-O99 = 1.902(6) Å and Sb2-O99 = 1.916(6) Å, whereas in previously reported cases, they fall in the range of 1.967(4)-1.986(4) Å.

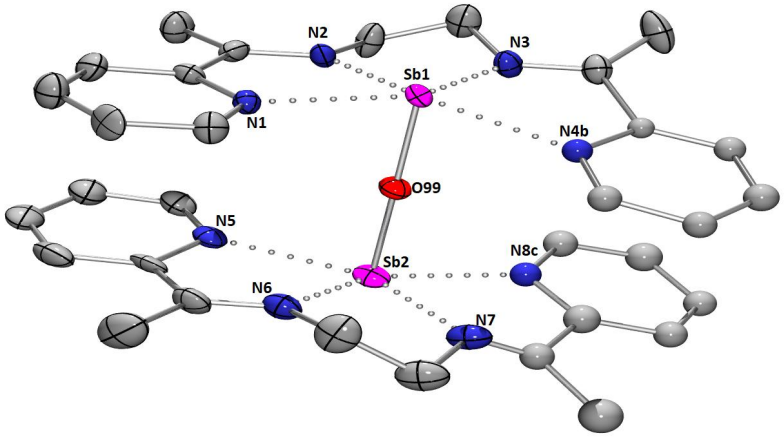

Figure 10. Molecular structure of the cationic part of **6** in the solid state (thermal ellipsoids at 30%, H atoms and counter anions are omitted for clarity). Selected bond lengths [Å] and angle [º]: Sb1-N1 = 2.481(7), Sb1-N2 = 2.286(7), Sb1-N3 = 2.266(8), Sb1-N4b = 2.46(3), Sb2-N5 = 2.479(8), Sb2-N6 = 2.283(8), Sb2-N7 = 2.283(9), Sb2-N8C = 2.36(3), Sb1-O99 = 1.902(6), Sb2-O99 = 1.916(6), Sb1-O99-Sb2 = 177.0(4).

Conclusion

In this study, we have stabilized tetra-cationic distibanes **[1]$_2$** and dismisthunaes **[2]$_2$** using tetra-coordinate bis-(alpha-iminopyridine) ligand **L**. Single crystal X-ray diffraction analysis reveals that **[1]$_2$** and **[2]$_2$** both have very labile Pn-Pn (Pn = Sb, Bi) bond due to Coulombic repulsion between two bonded Pn atoms. Compound **[1]$_2$** exhibits concentration-dependent colour changes in acetonitrile, and UV-Visible spectroscopy analysis indicates that this phenomenon stems from a labile Sb-Sb bond present in the compound **[1]$_2$**. Upon homolytic cleavage of the Sb-Sb bond, **[1]$_2$** generates a monomer radical (**[1]**$^{\cdot}$) in solution, establishing a monomer-dimer equilibrium. Using NMR and EPR spectroscopy, it has been demonstrated that this monomer species represents the first example of an **L**-stabilized Sb(II) di-cation radical (**[1]**$^{\cdot}$). Due to low stability of the monomer, it was not feasible to calculate monomer-dimer equilibrium constant. Reactivity studies further support the existence of the Sb(II) di-cation radical in the solution state, as all the observed reactions occurred at the antimony through homolytic cleavage of the Sb-Sb bond. Reactions with diphenyl dichalcogenides (Ph_2E-EPh_2) **[1]$_2$** led to generation of novel antimony-chalcogenide cations (LSb-EPh_2) (**3** and **4**). Furthermore, the reaction of **[1]$_2$** with 1,4-benzoquinone yielded compound **5**, while exposure to air or reaction with TEMPO resulted in the formation of oxo-bridged tetra-cationic species $[L_2(Sb^{2+})_2O](OTf)_4$ (**6**). Similarly, **[2]$_2$** has been characterized using UV-Visible and NMR spectroscopy, which indicate the presence of radicals in the solution state. These findings provide insights into the reactivity and structural properties of heavier dipnictane tetra-cations (Pn = Sb, Bi) and offer potential avenues for further exploration in the field of main group radical based catalysis and small molecule activation.

References

1) J. T. Boronski, A. E. Crumpton, L. L. Wales, S. Aldridge, *Science.* **2023**, *380*, 1147-1149.

2) S. P. Green, C. Jones, A. Stasch, *Science.* **2007**, *318*, 1754-1757.

3) a) D. E. Goldberg, D. H. Harris, M. F. Lappert, K. M. Thomas, *J.Chem. Soc. Chem. Commun.***1976**, 261; b) P. J. Davidson, D. H. Harris, M. F. Lappert, *J. Chem. Soc. Dalton Trans.* **1976**, 2268–2274; c) K. W. Klinkhammer, F. T. Fässler, H. Grützmacher, *Angew. Chem.* **1998**, *110*, 1142116; *Angew. Chem. Int. Ed.* **1998**, *37*, 1242126; d) P. P. Power, *Organometallics* **2007**, *26* ,4362–4372.

4) a) R. C. Fischer, P. P. Power, *Chem. Rev.* **2010**, 110, 3877–3923; b) Fischer, R. C., *Comprehensive Inorganic Chemistry II* **2013**, *1*, 269–287.

5) C. Jones, *Nat. Rev. Chem.* **2017**, *1*, 0059.

6) a) P. Power, *Nature* **2010**, *463*, 171-177; b) C. Weetman, *Chem. Eur. J.* **2021**, *27*, 1941-1954; c) Y. Pang, M. Leutzsch, N. Nöthling, J. Cornella, *Angew. Chem. Int. Ed.* **2023**, *62*, e2023020.

7) S. T. Liddle, Molecular Metal-Metal Bonds, Wiley-VCH, Weinheim, **2015**.

8) A. Gehlhaar, H. M. Weinert, C. Wölper, N. Semleit, G. Haberhauer, S. Schulz, *Chem. Commun.* **2022**, *58*, 6682-6685.

9) L. Weber, F. Ebeler, R. S. Ghadwal, *Coord. Chem. Rev.* **2022**, *461*, 214499.

10) D. Seyferth, *Organometallics* **2001**, *20*, 1488–1498.

11) a) F. A. Paneth, *Trans. Faraday Soc.* **1934**, *30*, 179–181; b) F. A. Paneth, H. Loleit, *J. Chem. Soc.* **1935**, 366–371; c) F. F. Blicke, U. O. Oakdale, F. D. Smith, *J. Am. Chem. Soc.*, **1931**, *53*, 1025-1029

12) a) G. Becker, H. Freudenblum, C. Witthauer, *Z. Anorg. Allg. Chem.* **1982**, *492*, 37–51; b) V. O. Mundt, G. Becker, M. Rössler, C. Witthauer, *Z. Anorg. Allg. Chem.* **1982**, *506*, 42-58.

13) a) O. Mundt, H. Riffel, G. Becker, A. Simon, *Z. Naturforsch. B* **1984**, *39*, 317–322; b) A. J. Ashe, E. G. Ludwig, J. Oleksyszyn, J. C. Huffman, *Organometallics* **1984**, *3*, 337–338; d) A. Kuczkowski, S. Heimann, A. Weber, S. Schulz, D. Bläser, C. Wölper, *Organometallics* **2011**, *30*, 4730–4735; e) P. Sharma, A. Cabrera, N. K. Jha, N. Rosas, R. Le Lagadec, M. Sharma, J. L. Arias, *Main Group Met. Chem.* **1997**, *20*, 697–710.

14) H. A. Meinema, C. J. R. C. Romão, J. G. Noltes, *J. Organomet. Chem.* **1973**, *55*, 139-141.

15) A. J. Ashe III, E. G. Ludwig Jr., *Organometallics* **1982**, *1*,1408.

16) a) H. J. Breunig, R. Kaller, A. Silvestru, *Phosphorus Sulfur Silicon Relat. Elem.* **1994**, *91*,165–168; b) L. Balazs, H. J. Breunig, E. Lork, A. Soran, C. Silvestru, *Inorg. Chem.* **2006**, *45*, 2341 – 2342.

17) S. Ishida, F. Hirakawa, K. Furukawa, K. Yoza, T. Iwamoto, *Angew. Chem. Int. Ed.* **2014**, *53*, 11172–11176; *Angew. Chem.* **2014**, *126*, 11354–11358.

18) R. J. Schwamm, M. P. Coles, *Chem. Eur. J.* **2019**, *25*, 14183–14191.

19) a) I. Vránová, M. Alonso, R. Jambor, A. Růžička, J. Turek, L. Dostál, *Chem. Eur. J.* **2017**, *23*, 2340–2349; b) P. Novák, M. Erben, R. Jambor, M. Hejda, A. Růžička, E. Rychagova, S. Ketkov, L. Dostál, *Dalton Trans.* **2023**, *52*, 218–227; c) T. Pugh, N. F. Chilton, R. A. Layfield, *Chem. Sci.* **2017**, *8*, 2073.

20) a) P. Pyykkö, *J. Phys. Chem. A* **2015**, *119*, 2326–2337; b) A. Bondi, *J. Phys. Chem.* **1964**, *68*, 441–451; c) Z. L. Wang, H. S. Hu, L. Szentpály, H. Stoll, S.Fritzsche, P. Pyykkö, W. H. E. Schwarz, J. Li, *Chem. Eur. J.* **2020**, *26*,15558–15564; d) J. P. Desclaux, *Data Nucl. Data Tables* **1973**,*12*, 311–406.

21) R. J. Schwamm, M. Lein, M. P. Coles, C. M. Fitchett, *Angew. Chem. Int. Ed.* **2016**, *55*, 14798–14801.

22) a) R. Kretschmer, D. A. Ruiz, C. E. Moore, A. L. Rheingold, G. Bertrand, *Angew. Chem. Int. Ed.* **2014**, *53*, 8176–8179; Angew. Chem. **2014**, *126*, 8315–8318; b) C. Helling, C. Wölper, G. E. Cutsail III, G. Haberhauer, S. Schulz, *Chem. Eur. J.* **2020**, *26*, 13390–13399; c) C. Helling, G. E. Cutsail III, H. Weinert, C. Wölper, S. Schulz, *Angew. Chem. Int. Ed.* **2020**, *59*, 7561–7568; *Angew. Chem.* **2020**, *132*, 7631–7638; d) C. Ganesamoorthy, C. Helling, C. Wölper, W. Frank, E. Bill, G. E.Cutsail III, S. Schulz, *Nat. Commun.* **2018**, *9*, 87–95; e) C. Helling, S. Schulz, *Eur. J. Inorg .Chem.* **2020**, 3209–3221.

23) a) H. M. Weinert, Y. Schulte, A. Gehlhaar, C. Wölper, G. Haberhauer, S. Schulz, *Chem. Commun.* **2023**, *59*, 7755-7758; b) A. Barthélemy, H. Scherer, M. Daub, A. Bugnet, I. Krossing, *Angew. Chem. Int. Ed.* **2023**, *62*, e2023116. c) A. Barthélemy, H. Scherer, H. Weller, I. Krossing, *Chem. Commun.* **2023**, *59*, 1353–1356; d) S. Yao, A. Kostenko, Y. Xiong, C. Lorent, A. Ruzicka, M. Driess, *Angew. Chem. Int. Ed.* **2021**, *60*, 14864–14868; *Angew. Chem.* **2021**, *133*, 14990–14994;

24) S. Biswas, N. Patel, R. Deb, M. Majumdar, *Chem. Rec.* **2022**, *22*, e202200003.

25) a) R. K. Raut, M. Majumdar, *Chem. Commun.* **2017**, *53*, 1467–1469; b) M. Majumdar, R. K. Raut, P. Sahoo, V. Kumar, *Chem. Commun.* **2018**, *54*,10839–10842.

26) H. Haldar, C. B. Yildiz, M. Majumdar *ChemPlusChem* **2023**, *88*, e202300211.

27) S. Banerjee, J. Gangopadhyay, C.-Z. Lu, J.-T. Chen, A. Ghosh, *Eur.J. Inorg. Chem.* **2004**, 2533.

28) T. Sasamori, E. Mieda, N. Nagahora, K. Sato, D. Shimoi, T. Takui, Y. Hosoi, Y. Furukawa, N. Tagaki, S. Nagase, N. Tokitoh, *J. Am. Chem. Soc.* **2006**, *128*, 12582 – 12588.

29) a) H. J. Breunig, S. Gülec, *Z. Naturforsch.* **1986**, *41b,* 1387-1390; b) H. J. Breunig, H. Jawad, *J. Organomet. Chem.* **1984**, *277*, 257-260.

30) L. Le, S. Li, D. Zhang, S.-F. Yin, N. Kambe, R. Qiu, *Org. Lett.* **2022**, *24*, 6159−6164.

31) F. Geist, S. Martínez, J. Ramler, K. Oberdorf, L. Brändler, S. Reith, C. Lichtenberg, *Eur. J. Inorg. Chem.* **2023**, *26*, e202300415.

32) T. Li, H. Wei, Y. Fang, L. Wang, S. Chen, Z. Zhang, Y. Zhao, G. Tan, X. Wang, *Angew. Chem. Int. Ed.* **2017**, *56*, 632–636.

33) H. J. Breunig, T. Krüger, E. Lork, *J. Organomet. Chem.* **2002**, *648*, 209-213.

34) H. J. Breunig, T. Krüger, E. Lork, *Angew. Chem.* **1997**, *109*, 654; *Angew. Chem. Int. Ed. Engl.* **1997**, *36*, 615.

Appendix

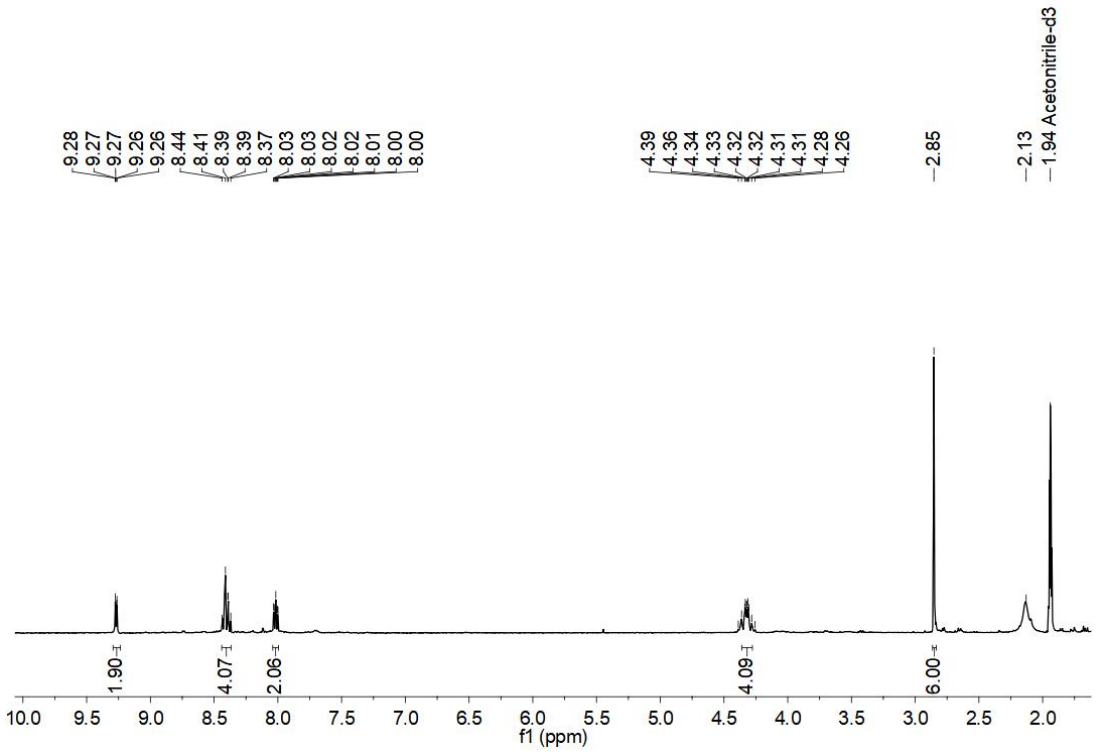

Figure S1. ^{1}H NMR spectrum (400 MHz, CD_3CN, 298 K, 2.91 mM) of **[1]**$_2$.

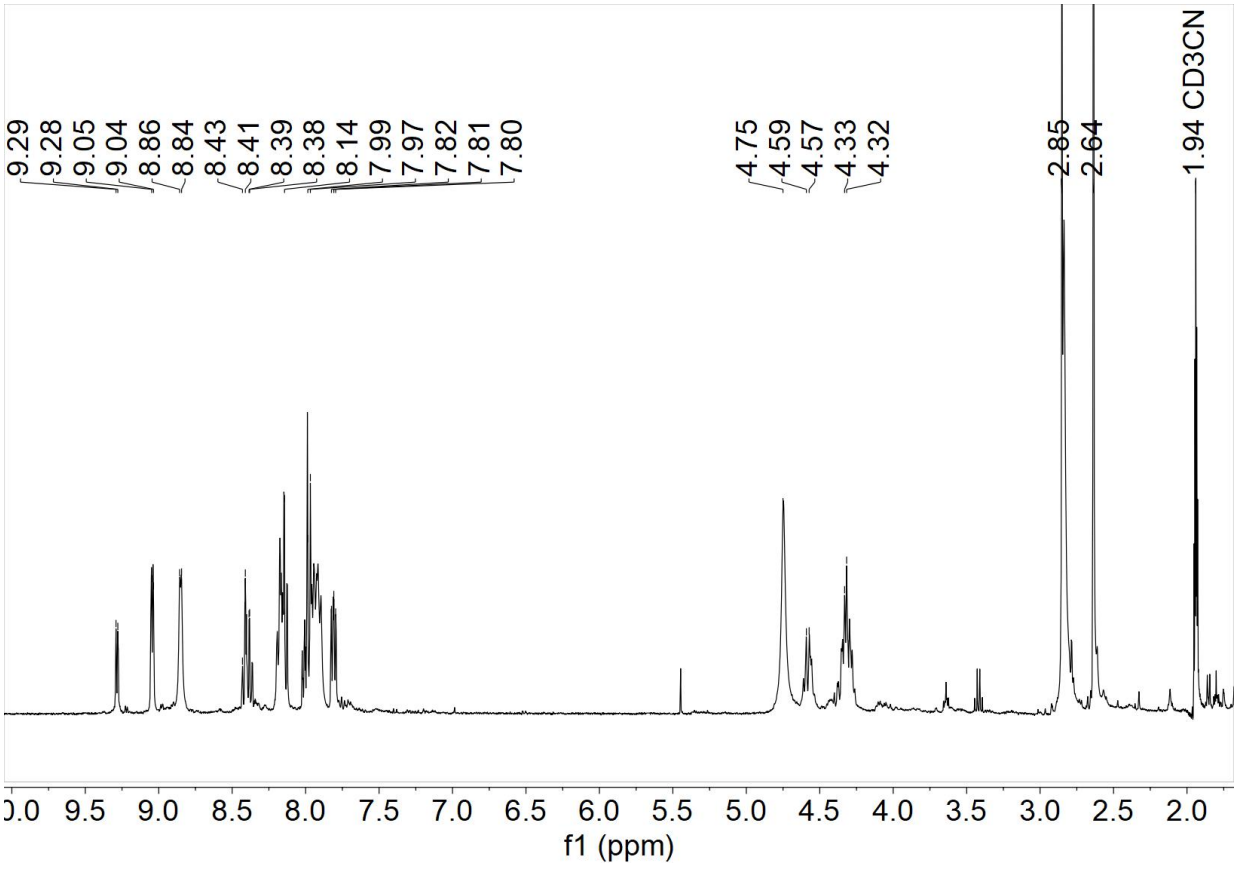

Figure S2. ^{1}H NMR spectrum (400 MHz, CD_3CN, 298 K, 32.78 mM) of **[1]**$_2$.

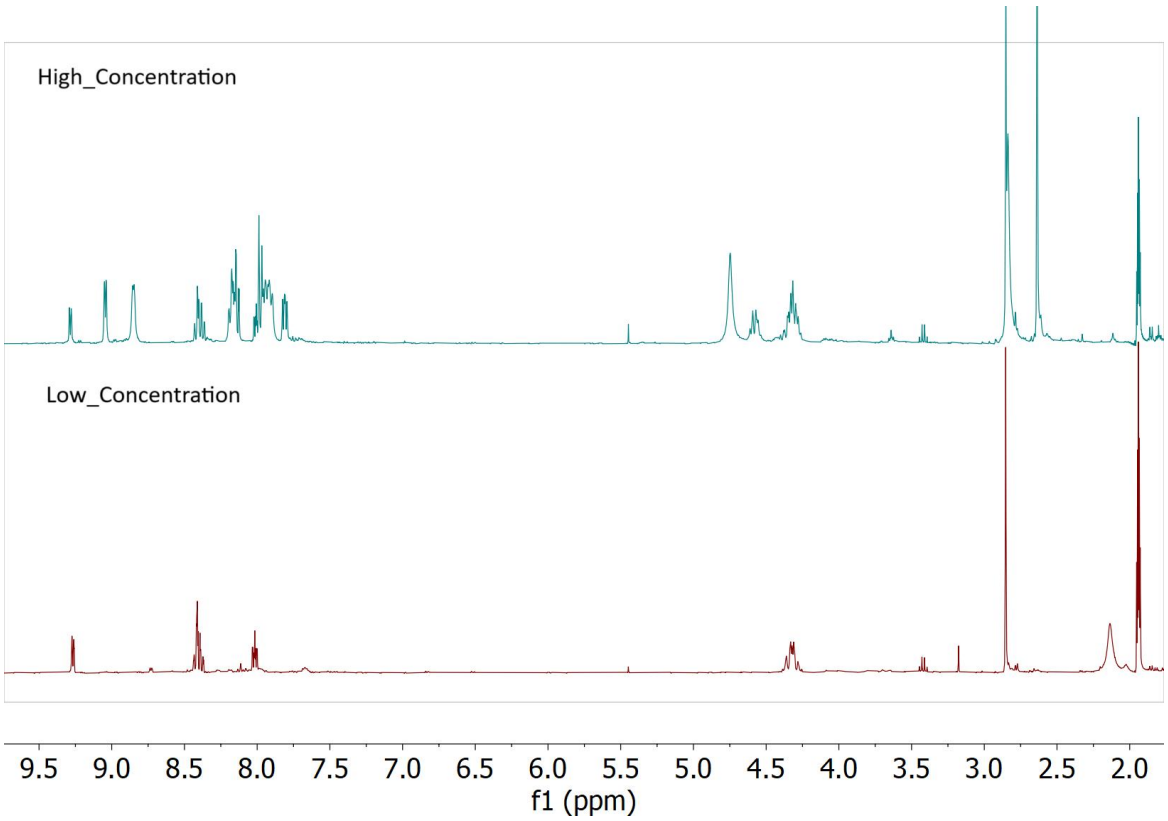

Figure S3 Stacked ^{1}H NMR spectra of **[1]$_2$** in two different concentrations : (400 MHz, CD_3CN, 298 K, 2.91 mM) and (400 MHz, CD_3CN, 298 K, 32.78 mM).

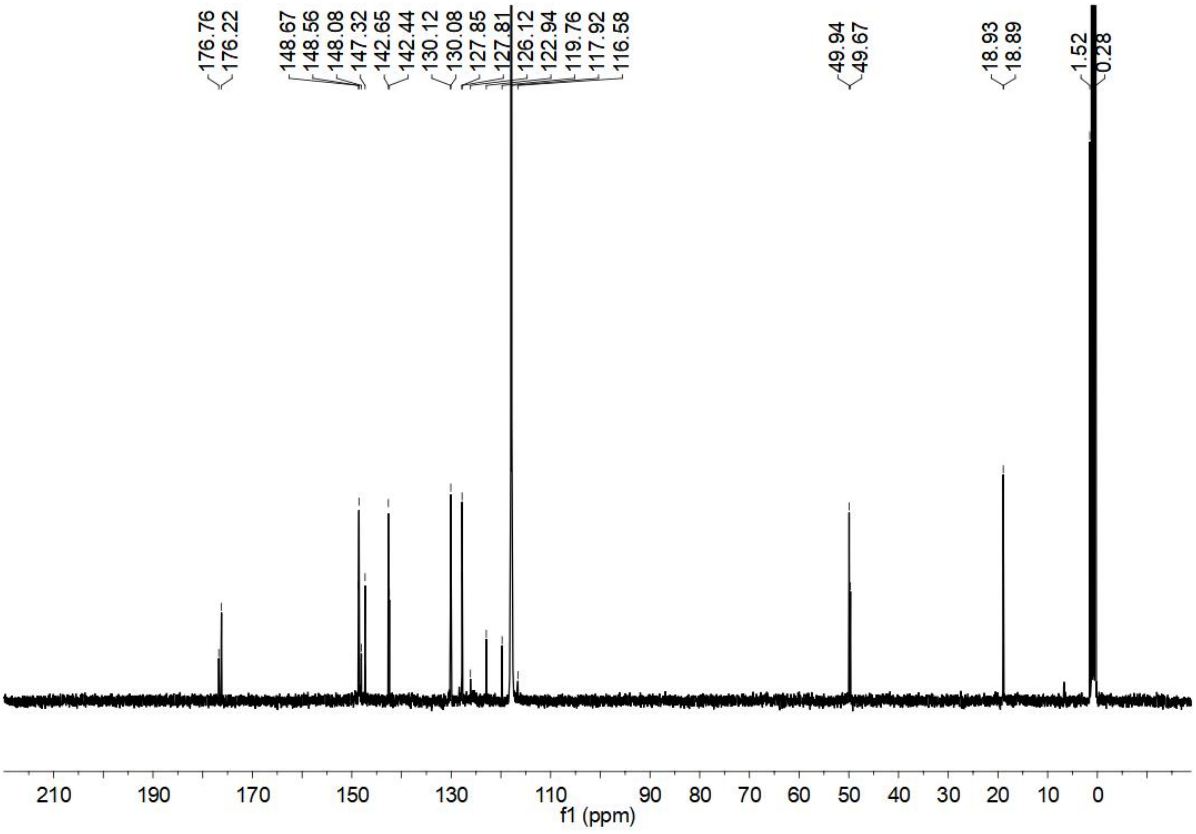

Figure S4. $^{13}C\{^{1}H\}$ NMR spectrum (101 MHz, $CDCl_3$, 298 K, 32.78 mM) of **[1]$_2$**.

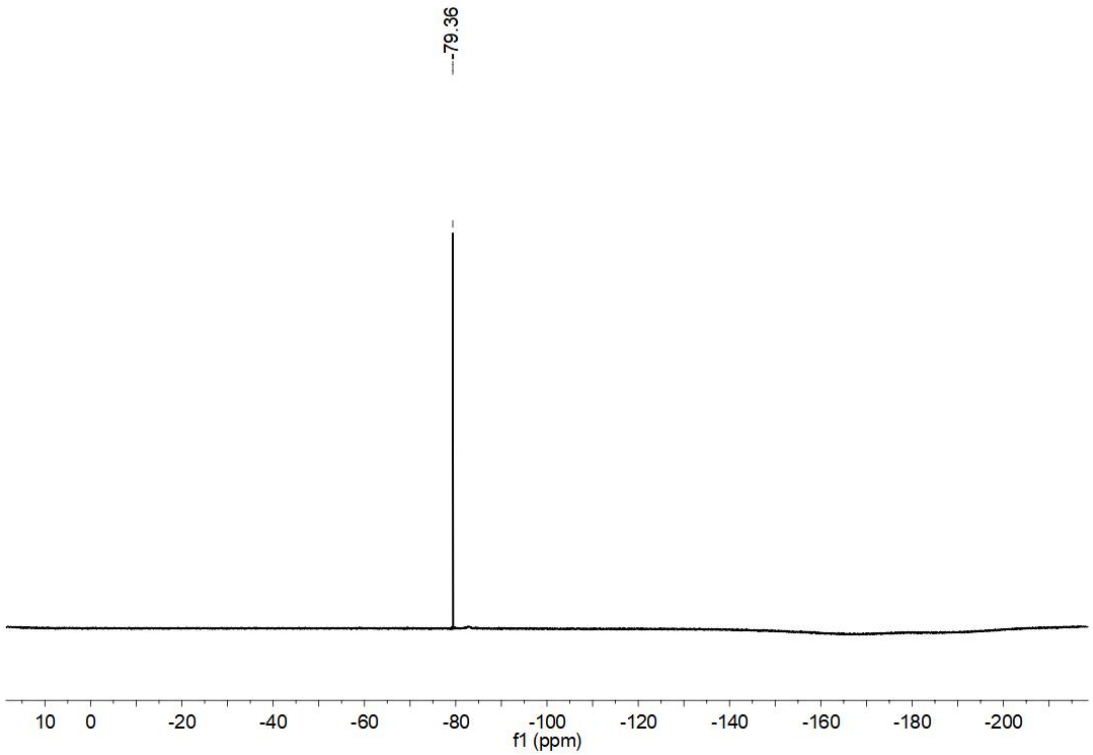

Figure S5. $^{19}F\{^{1}H\}$ NMR spectrum (377 MHz, CD_3CN, 298 K) of **[1]$_2$**.

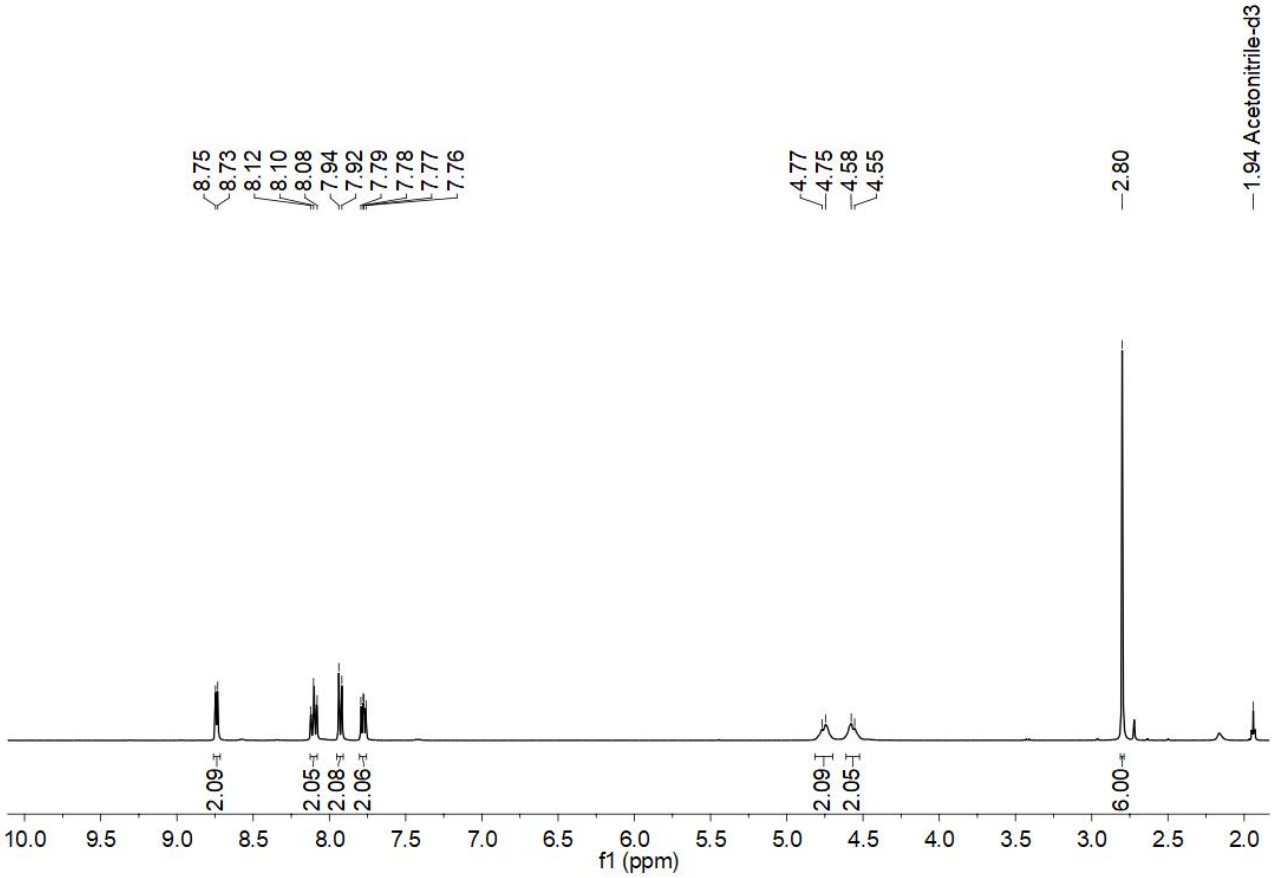

Figure S6. ^{1}H NMR spectrum (400 MHz, CD_3CN, 298 K, 16.16 mM) of **[2]$_2$**.

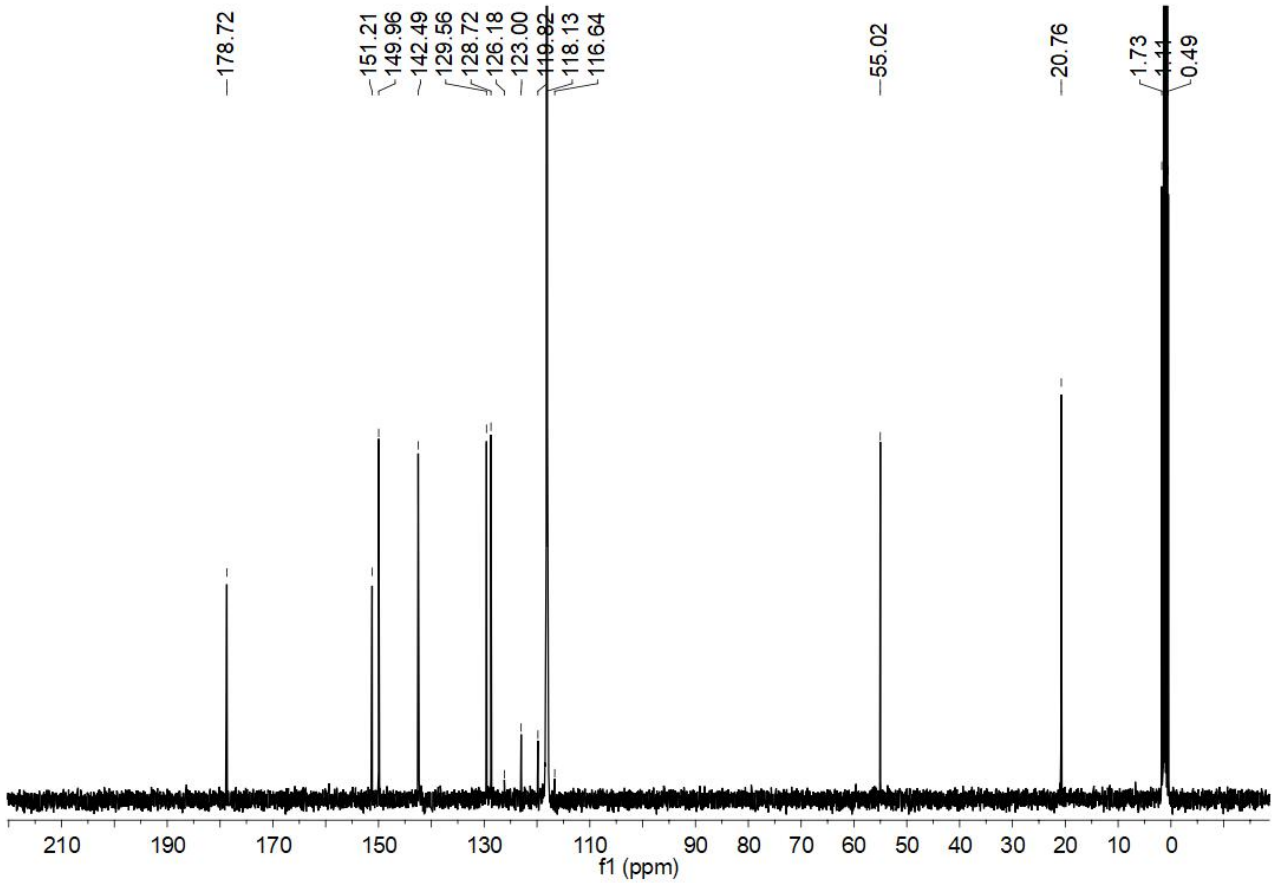

Figure S7. $^{13}C\{^{1}H\}$ NMR spectrum (101 MHz, $CDCl_3$, 298 K, 16.16 mM) of **[2]$_2$**.

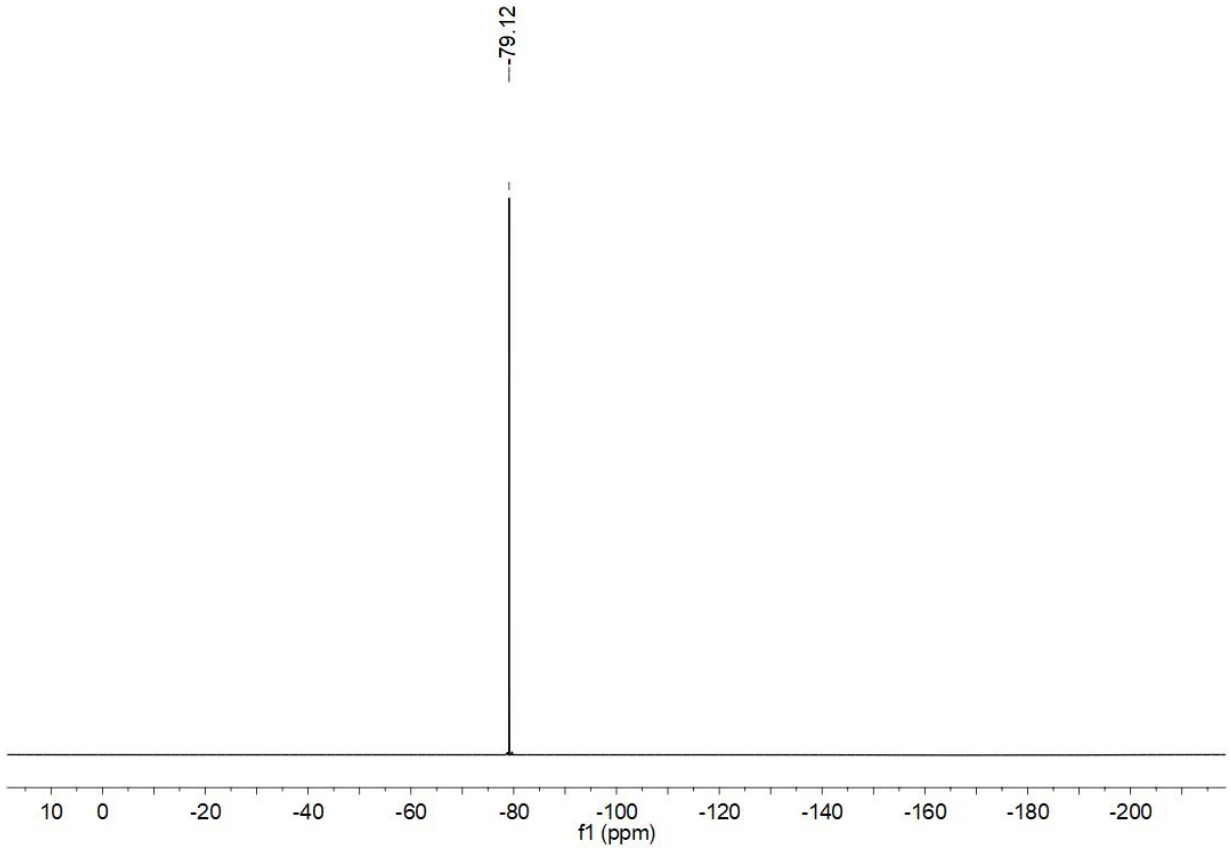

Figure S8. 19 $^{19}F\{^{1}H\}$ NMR spectrum (377 MHz, CD_3CN, 298 K) of **[2]$_2$**.

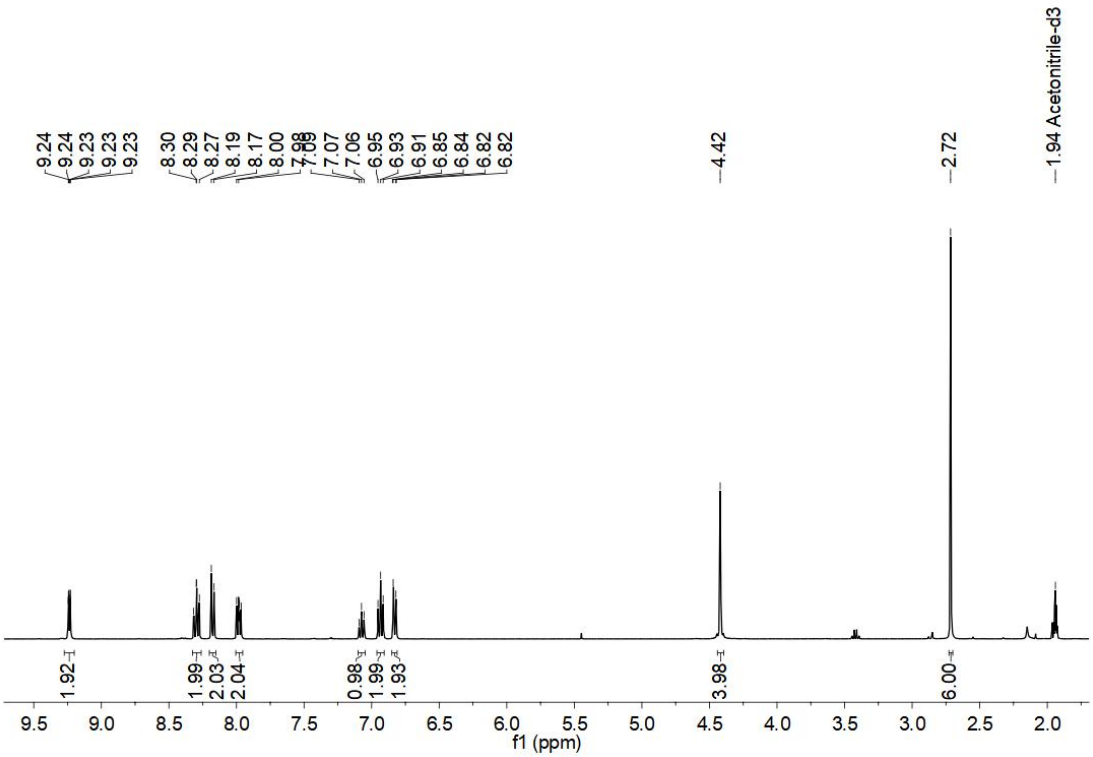

Figure S9. ^{1}H NMR spectrum (400 MHz, CD_3CN, 298 K) of **3**.

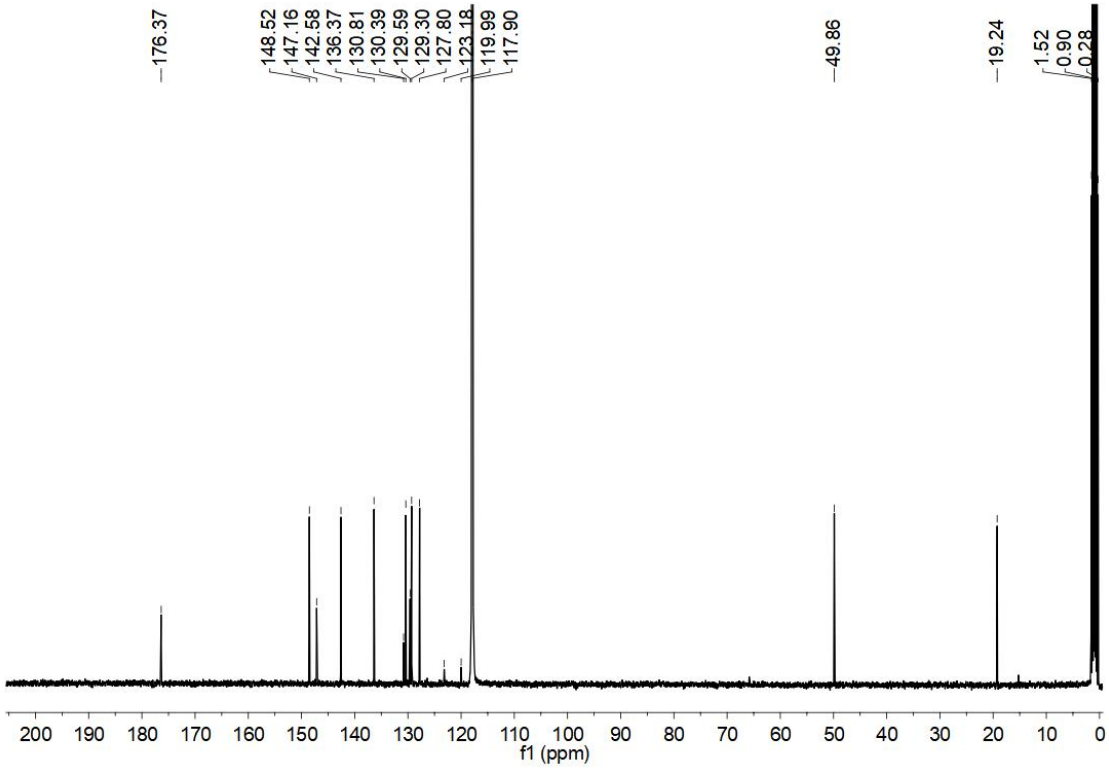

Figure S10. $^{13}C\{^{1}H\}$ NMR spectrum (101 MHz, CD_3CN, 298 K) of **3**.

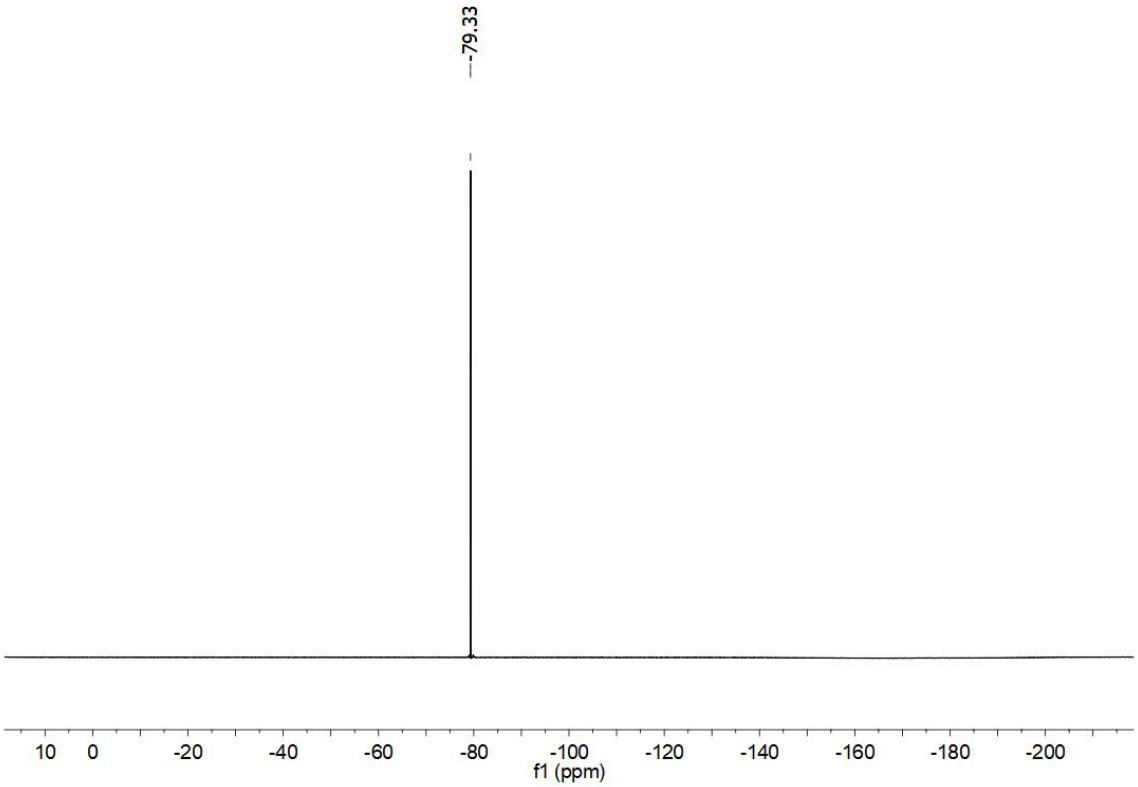

Figure S11. $^{19}F\{^{1}H\}$ NMR spectrum (377 MHz, CD_3CN, 298 K) of **3**.

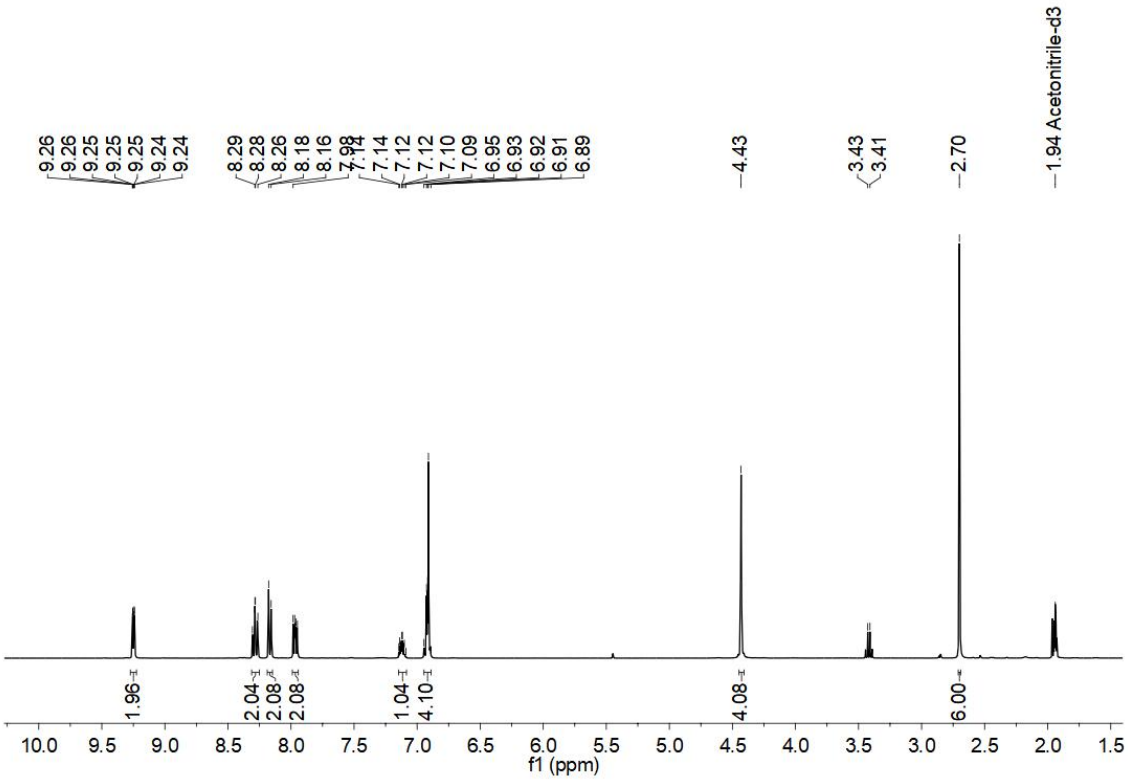

Figure S12. ^{1}H NMR spectrum (400 MHz, CD_3CN, 298 K) of **4**.

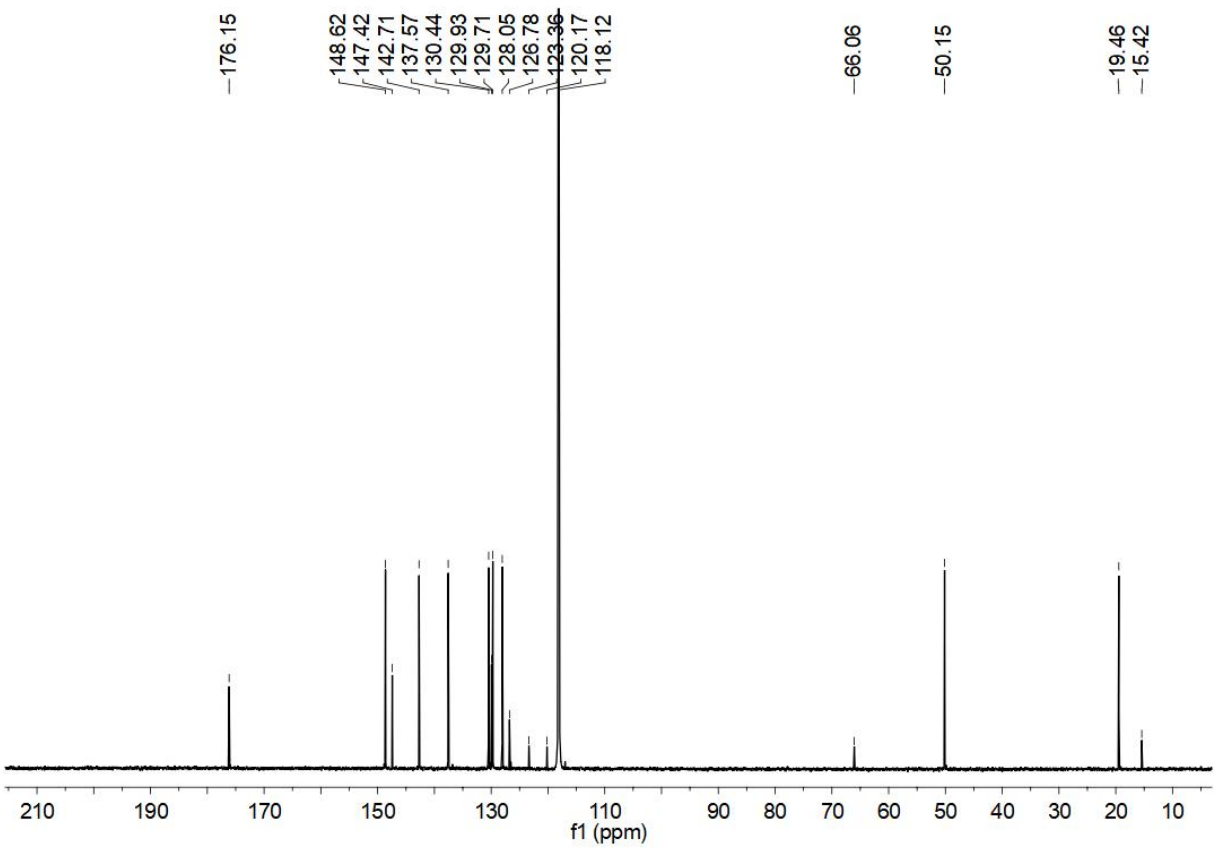

Figure S13. $^{13}C\{^{1}H\}$ NMR spectrum (101 MHz, CD_3CN, 298 K) of **4**.

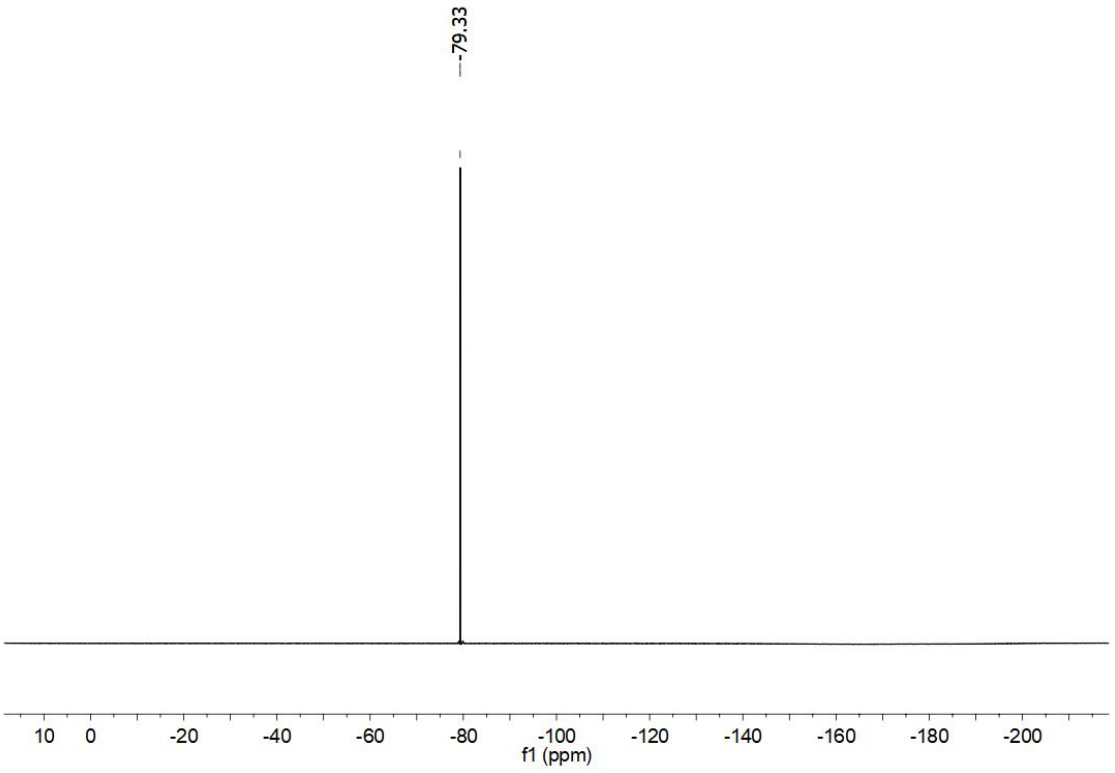

Figure S14. $^{19}F\{^{1}H\}$ NMR spectrum (377 MHz, CD_3CN, 298 K) of **4**.

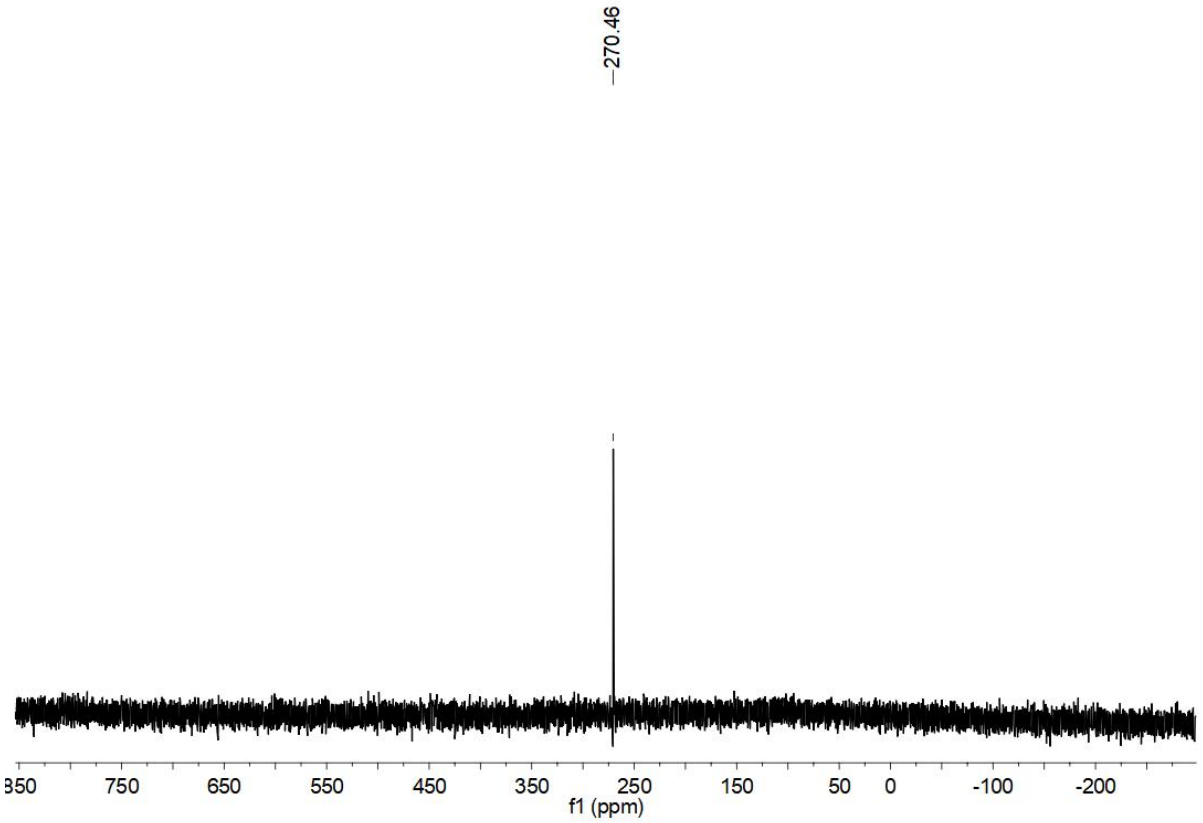

Figure S15. ^{77}Se NMR spectrum (377 MHz, CD_3CN, 298 K) of **4**.

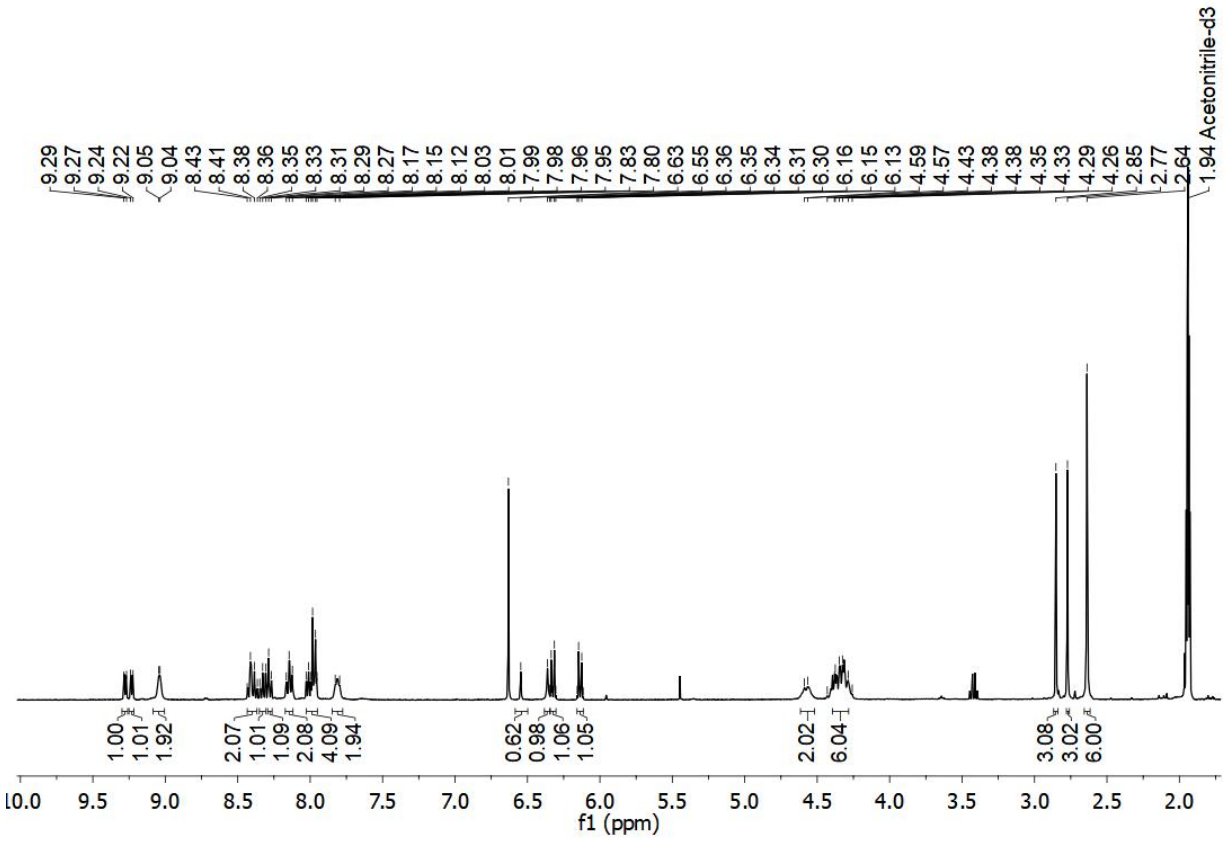

Figure S16. ^{1}H NMR spectrum (400 MHz, CD_3CN, 298 K) of **5**.

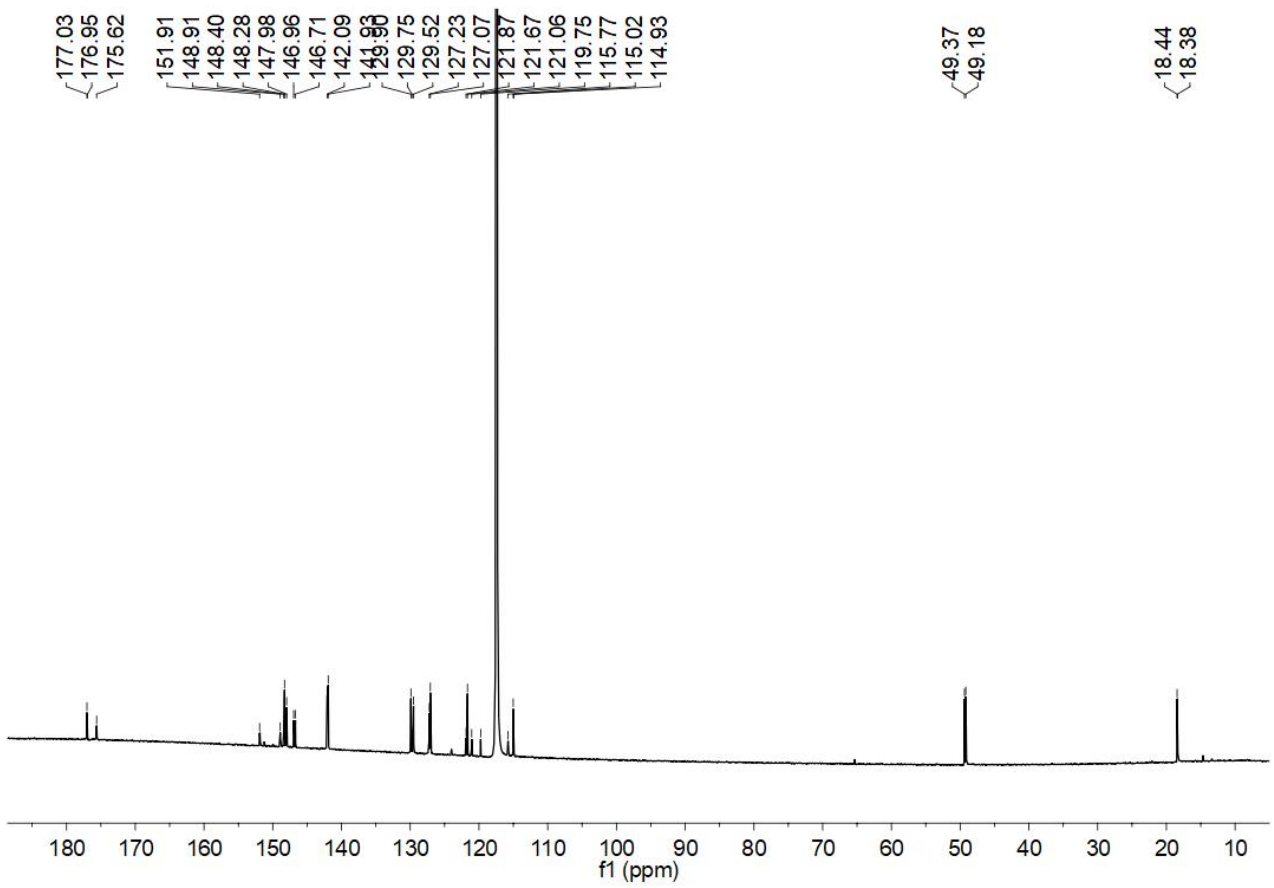

Figure S17. $^{13}C\{^{1}H\}$ NMR spectrum (101 MHz, CD_3CN, 298 K) of **5**.

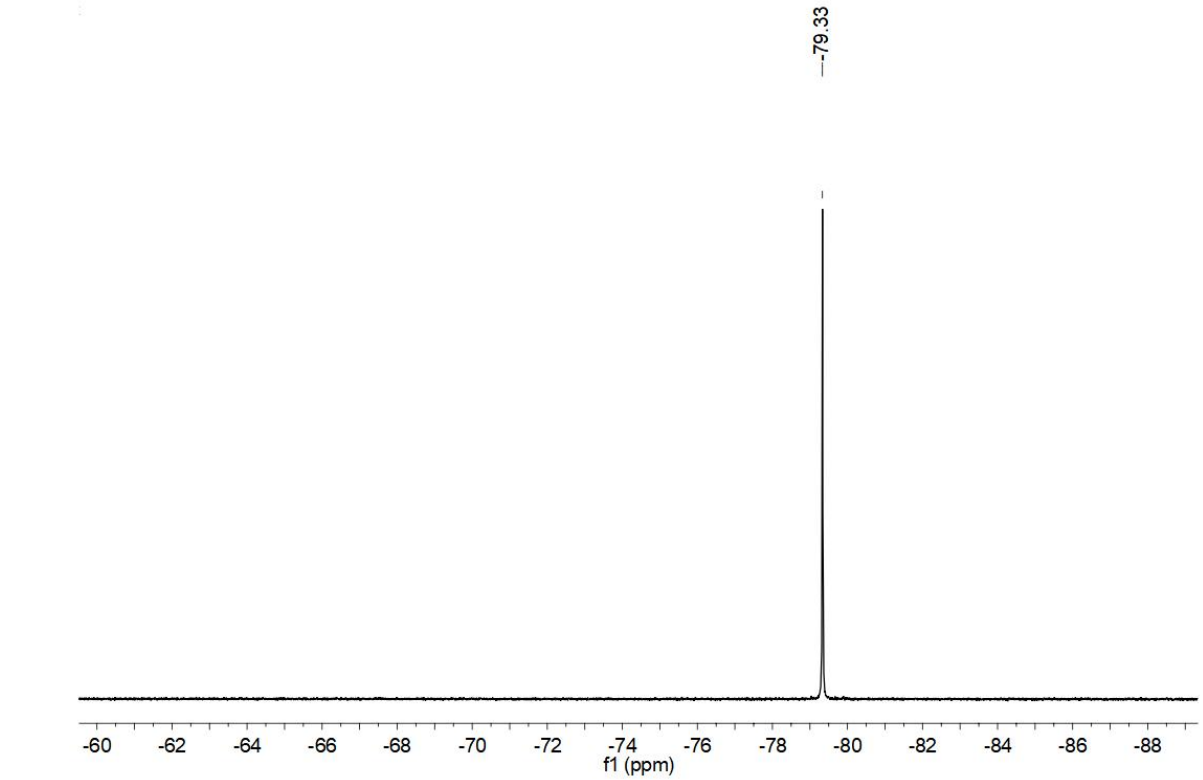

Figure S18. $^{19}F\{^{1}H\}$ NMR spectrum (377 MHz, CD_3CN, 298 K) of **5**.

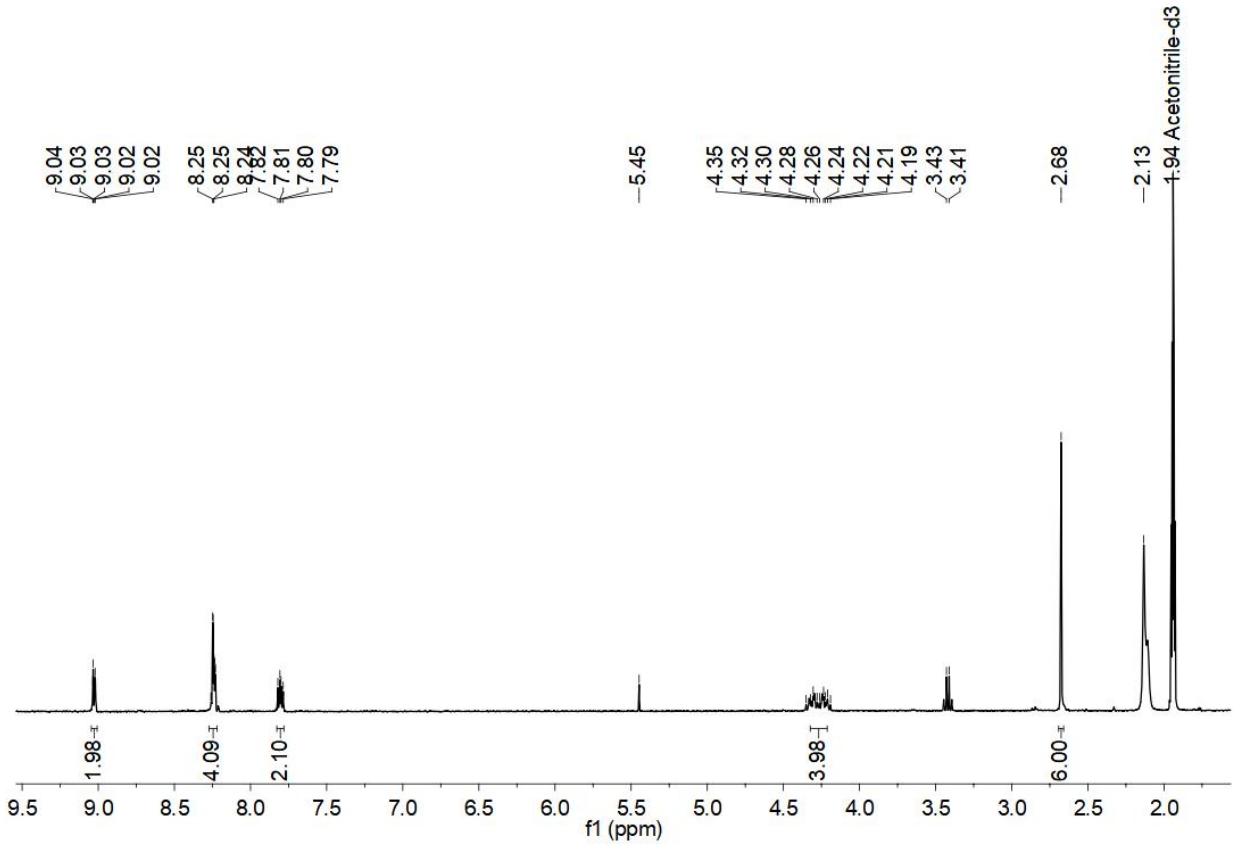

Figure S19. ^{1}H NMR spectrum (400 MHz, CD_3CN, 298 K) of **6**.

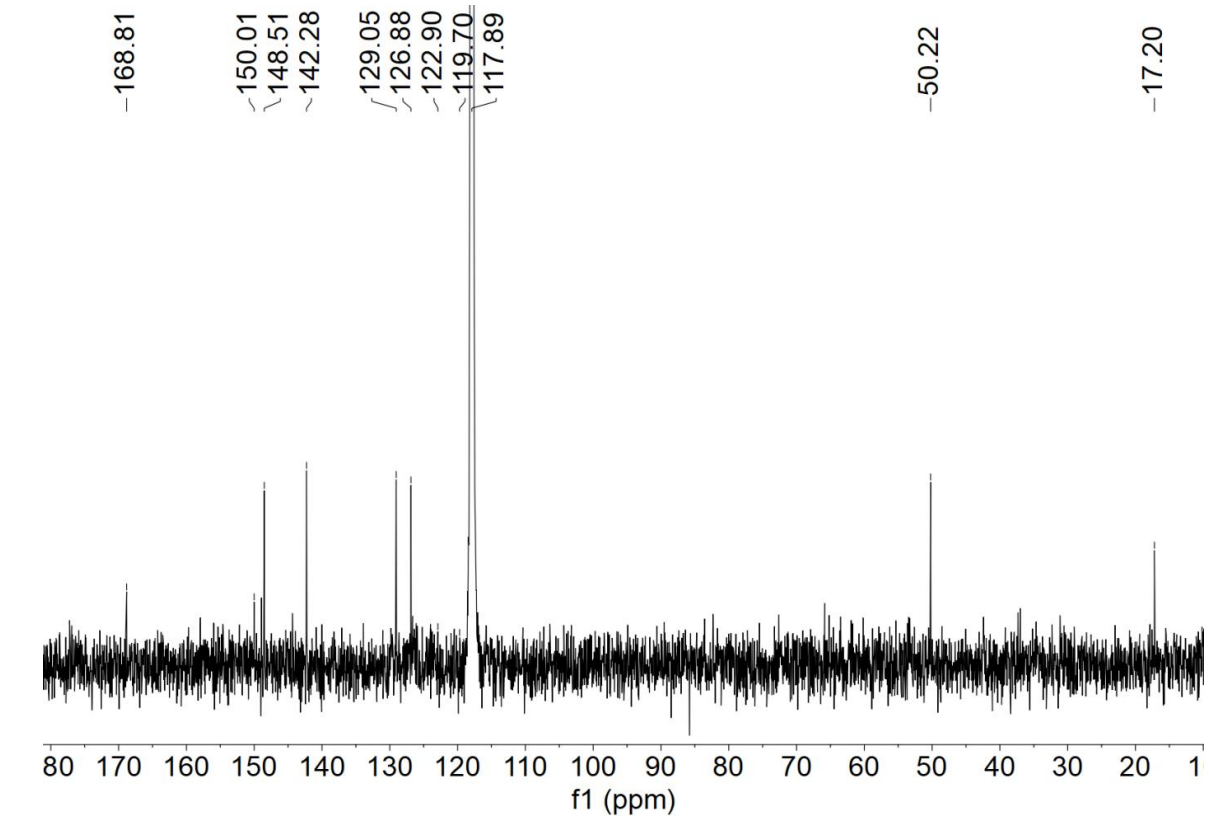

Figure S20. $^{13}C\{^{1}H\}$ NMR spectrum (101 MHz, CD_3CN, 298 K) of **6**.

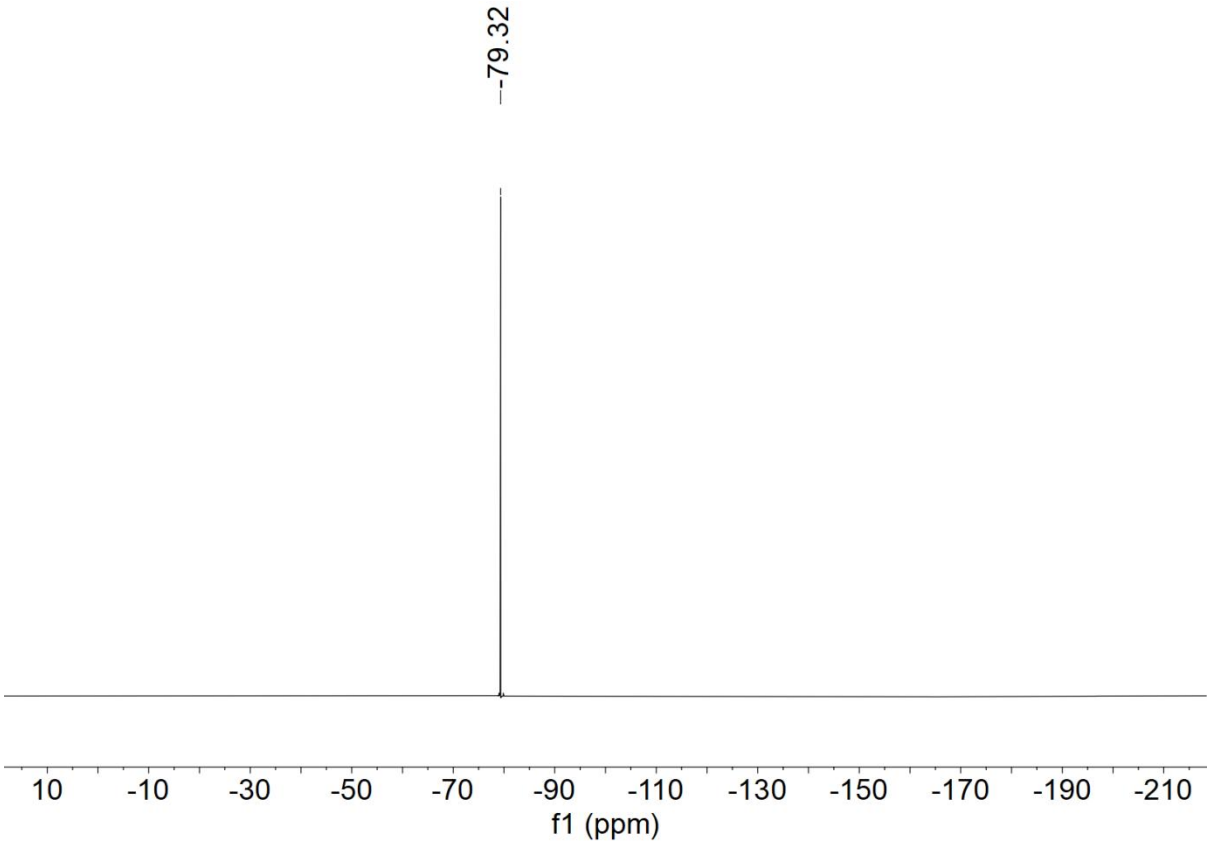

Figure S21. $^{19}F\{^{1}H\}$ NMR spectrum (377 MHz, CD_3CN, 298 K) of **6**.

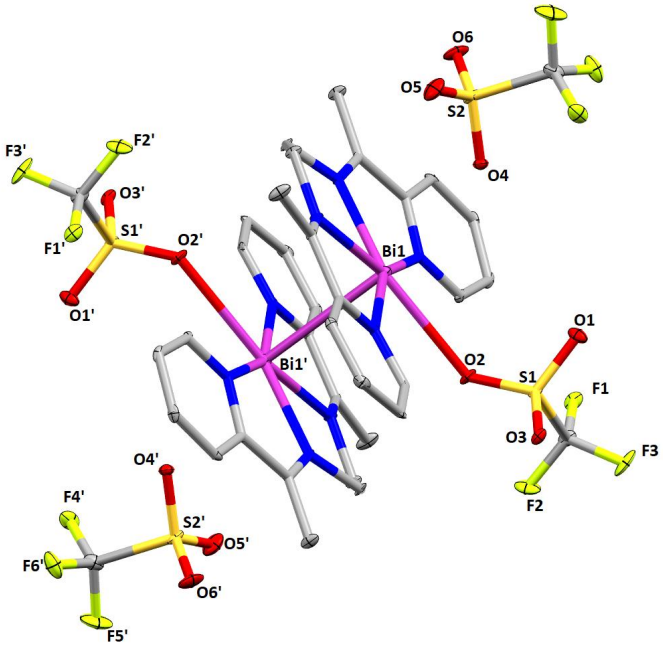

Figure S22. Molecular structure of the cationic fully grown **[2]$_2$** in the solid state (thermal ellipsoids at 30%, H atoms and counter anions are omitted for clarity). Selected bond lengths [Å]: Bi1-O2 = Bi1'-O2' = 2.774(4), Bi1-O4 = Bi1'-O4' = 3.025(6).

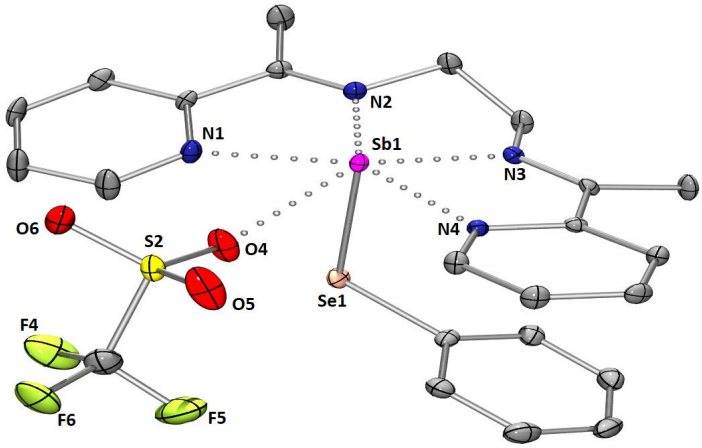

Figure S23. Molecular structure of the [LSb-SePh(OTf)] cationic part of **4** in the solid state (thermal ellipsoids at 30%, H atoms and counter anions are omitted for clarity). Selected bond lengths [Å]: Sb1-N1 = 2.561(3), Sb1-N2 = 2.333(2), Sb1-N3 = 2.240(3), Sb1-N4 = 2.434(2), Sb1-Se1 = 2.5595(5), Sb1-O4 = 2.858(2).

Table 1: Crystal data and structure refinement for **[1]$_2$**

Empirical formula	C3.6 H3.8 F1.1 N0.9 O1.1 S0.4 Sb0.2	
Formula weight	215.84	
Temperature	296.15 K	
Wavelength	0.71073 Å	
Crystal system	Monoclinic	
Space group	$P2_1/c$	
Unit cell dimensions	a = 10.856(5) Å	α= 90°.
	b = 21.630(10) Å	β = 95.461(9)°.
	c = 23.041(10) Å	γ = 90°.
Volume	5386(4) Å^3	
Z	44	
Density (calculated)	2.928 Mg/m^3	
Absorption coefficient	5.937 mm^{-1}	
F(000)	4312	
Crystal size	0.184 x 0.167 x 0.109 mm^3	
Theta range for data collection	1.294 to 25.068°.	
Index ranges	-12<=h<=12, -25<=k<=25, -27<=l<=27	
Reflections collected	43358	
Independent reflections	9515	
Completeness to theta = 25.213°	99.7 %	
Absorption correction	multi-scan	
Max. and min. transmission	0.7452 and 0.6459	
Refinement method	Full-matrix least-squares on F^2	
Data / restraints / parameters	9515 / 0 / 727	
Goodness-of-fit on F^2	1.862	
Final R indices [I>2sigma(I)]	R1 = 0.1281, wR2 = 0.3366	
R indices (all data)	R1 = 0.1850, wR2 = 0.3551	
Largest diff. peak and hole	2.142 and -2.455 e.Å^{-3}	

Table 2: Crystal data and structure refinement for **[2]$_2$**

Empirical formula	C18 H18 Bi F6 N4 O6 S2	
Formula weight	773.46	
Temperature	296.15 K	
Wavelength	0.71073 Å	
Crystal system	Triclinic	
Space group	P-1	
Unit cell dimensions	a = 9.9873(11) Å	α= 110.505(2)°.
	b = 11.0965(11) Å	β = 98.097(2)°.
	c = 11.7760(12) Å	γ = 93.889(3)°.
Volume	1200.5(2) Å^3	
Z	2	
Density (calculated)	2.140 Mg/m^3	
Absorption coefficient	7.608 mm^{-1}	
F(000)	742	
Crystal size	0.116 x 0.083 x 0.07 mm^3	
Theta range for data collection	1.876 to 25.081°.	
Index ranges	-9<=h<=11, -13<=k<=13, -14<=l<=14	
Reflections collected	14394	
Independent reflections	4246	
Completeness to theta = 25.213°	99.7 %	
Absorption correction	multi-scan	
Max. and min. transmission	0.7452 and 0.5746	
Refinement method	Full-matrix least-squares on F^2	
Data / restraints / parameters	4246 / 0 / 340	
Goodness-of-fit on F^2	1.068	
Final R indices [I>2sigma(I)]	R1 = 0.0373, wR2 = 0.0830	
R indices (all data)	R1 = 0.0485, wR2 = 0.0871	
Largest diff. peak and hole	1.632 and -1.287 e.Å^{-3}	

Table 3: Crystal data and structure refinement for **3**

Empirical formula	C48 H46 F12 N8 O12 S6 Sb2	
Formula weight	1590.79	
Temperature	296.15 K	
Wavelength	0.71073 Å	
Crystal system	Triclinic	
Space group	P-1	
Unit cell dimensions	a = 9.9464(13) Å	α= 61.121(3)°.
	b = 13.0826(16) Å	β = 77.370(4)°.
	c = 13.4016(18) Å	γ = 85.237(4)°.
Volume	1489.5(3) $Å^3$	
Z	1	
Density (calculated)	1.773 Mg/m^3	
Absorption coefficient	1.220 mm^{-1}	
F(000)	792	
Crystal size	0.252 x 0.17 x 0.146 mm^3	
Theta range for data collection	2.099 to 25.089°.	
Index ranges	-11<=h<=11, -15<=k<=15, -15<=l<=15	
Reflections collected	29945	
Independent reflections	5292	
Completeness to theta = 25.213°	99.8 %	
Absorption correction	multi-scan	
Max. and min. transmission	0.7452 and 0.5936	
Refinement method	Full-matrix least-squares on F^2	
Data / restraints / parameters	5292 / 10 / 436	
Goodness-of-fit on F^2	1.063	
Final R indices [I>2sigma(I)]	R1 = 0.0239, wR2 = 0.0523	
R indices (all data)	R1 = 0.0302, wR2 = 0.0549	
Largest diff. peak and hole	0.444 and -0.501 $e.Å^{-3}$	

Table 4: Crystal data and structure refinement for **4**

Empirical formula	C12.62 H12.44 F3 N2.31 O3 S Sb0.50 Se0.50	
Formula weight	433.98	
Temperature	296.15 K	
Wavelength	0.71073 Å	
Crystal system	Triclinic	
Space group	P-1	
Unit cell dimensions	a = 13.4743(12) Å	α= 78.971(3)°.
	b = 15.3311(14) Å	β = 79.877(3)°.
	c = 16.2844(15) Å	γ = 73.964(3)°.
Volume	3146.3(5) $Å^3$	
Z	8	
Density (calculated)	1.832 Mg/m^3	
Absorption coefficient	2.250 mm^{-1}	
F(000)	1711	
Crystal size	0.27 x 0.194 x 0.132 mm^3	
Theta range for data collection	1.907 to 25.087°.	
Index ranges	-16<=h<=15, -18<=k<=18, -19<=l<=19	
Reflections collected	63727	
Independent reflections	11161	
Completeness to theta = 25.213°	99.7 %	
Absorption correction	multi-scan	
Max. and min. transmission	0.7452 and 0.5732	
Refinement method	Full-matrix least-squares on F^2	
Data / restraints / parameters	11161 / 0 / 797	
Goodness-of-fit on F^2	1.011	
Final R indices [I>2sigma(I)]	R1 = 0.0306, wR2 = 0.0650	
R indices (all data)	R1 = 0.0440, wR2 = 0.0701	
Largest diff. peak and hole	0.688 and -0.567 $e.Å^{-3}$	

Table 5: Crystal data and structure refinement for **5**

Empirical formula	C46 H46 F12 N10 O14 S4 Sb2	
Formula weight	1562.67	
Temperature	293(2) K	
Wavelength	0.71073 Å	
Crystal system	Triclinic	
Space group	P-1	
Unit cell dimensions	a = 10.6785(13) Å	α= 109.093(3)°.
	b = 11.9818(16) Å	β = 97.456(4)°.
	c = 12.2438(16) Å	γ = 97.922(4)°.
Volume	1440.4(3) $Å^3$	
Z	1	
Density (calculated)	1.801 Mg/m^3	
Absorption coefficient	1.194 mm^{-1}	
F(000)	778	
Crystal size	0.151 x 0.139 x 0.113 mm^3	
Theta range for data collection	1.960 to 25.077°.	
Index ranges	-12<=h<=12, -14<=k<=14, -14<=l<=14	
Reflections collected	39288	
Independent reflections	5122	
Completeness to theta = 25.213°	99.9 %	
Absorption correction	multi-scan	
Max. and min. transmission	0.7452 and 0.4906	
Refinement method	Full-matrix least-squares on F^2	
Data / restraints / parameters	5122 / 752/ 448	
Goodness-of-fit on F^2	1.046	
Final R indices [I>2sigma(I)]	R1 = 0.0427, wR2 = 0.1012	
R indices (all data)	R1 = 0.0486, wR2 = 0.1063	
Largest diff. peak and hole	1.037 and -1.169 $e.Å^{-3}$	

Table 6: Crystal data and structure refinement for **6**

Empirical formula	C38.50 H36 F12 N9.25 O13 S4 Sb2	
Formula weight	1436.00	
Temperature	293(2) K	
Wavelength	0.71073 Å	
Crystal system	monoclinic	
Space group	C2/c	
Unit cell dimensions	a = 22.029(8) Å	α= 90°.
	b = 20.912(7) Å	β = 98.126(14)°.
	c = 23.412(11) Å	γ = 90°.
Volume	10677(7) $Å^3$	
Z	8	
Density (calculated)	1.787 Mg/m^3	
Absorption coefficient	1.278 mm^{-1}	
F(000)	5678	
Crystal size	0.126 x 0.095 x 0.073 mm^3	
Theta range for data collection	1.349 to 25.160°.	
Index ranges	-26<=h<=26, -24<=k<=24, -27<=l<=27	
Reflections collected	70091	
Independent reflections	9495	
Completeness to theta = 25.213°	99.2 %	
Absorption correction	multi-scan	
Max. and min. transmission	0.7452 and 0.6596	
Refinement method	Full-matrix least-squares on F^2	
Data / restraints / parameters	9495 / 2269/ 974	
Goodness-of-fit on F^2	1.118	
Final R indices [I>2sigma(I)]	R1 = 0.0699, wR2 = 0.1393	
R indices (all data)	R1 = 0.1212, wR2 = 0.1599	
Largest diff. peak and hole	1.101 and -0.962 $e.Å^{-3}$	